A genetically-encoded toolkit of functionalized nanobodies against fluorescent proteins for visualizing and manipulating intracellular signalling

David L. Prole[1,*] and Colin W. Taylor[1,*]

[1]Department of Pharmacology, University of Cambridge, Tennis Court Road, Cambridge CB2 1PD, United Kingdom

[*]**For correspondence**: dp350@cam.ac.uk, cwt1000@cam.ac.uk

Short title

Functionalized nanobodies for studying intracellular signalling

Keywords: cell signalling, endoplasmic reticulum, fluorescence microscopy, fluorescent protein, GFP, intrabody, membrane contact site, mitochondria, nanobody, RFP.

Abbreviations

BFP, blue fluorescent protein; $[Ca^{2+}]_c$, cytosolic free Ca^{2+} concentration; CALI, chromophore-assisted light inactivation; CaM, calmodulin; CFP, cyan fluorescent protein; ER, endoplasmic reticulum; FKBP, FK506-binding protein; FRB, FKBP-rapamycin-binding domain; FP, fluorescent protein; GFP, green fluorescent protein; GNab, GFP-binding nanobody; HBS, HEPES-buffered saline; IP_3R, inositol 1,4,5-trisphosphate receptor; LAMP1, lysosomal membrane protein 1; mCherry, monomeric Cherry; MCS, membrane contact site; MHBS, modified HBS; MP, multimerizing protein; mRFP, monomeric red fluorescent protein; OMM, outer mitochondrial membrane; PM, plasma membrane; RFP, red fluorescent protein; RNab, RFP-binding nanobody; ROI, region of interest; SOCE, store-operated Ca^{2+} entry; TIRFM, total internal reflection fluorescence microscopy; YFP, yellow fluorescent protein.

Abstract

Background: Intrabodies enable targeting of proteins in live cells, but it remains a huge task to generate specific intrabodies against the thousands of proteins in a proteome. We leverage the widespread availability of fluorescently labelled proteins to visualize and manipulate intracellular signalling pathways in live cells by using nanobodies targeting fluorescent protein tags.

Results: We generated a toolkit of plasmids encoding nanobodies against red and green fluorescent proteins (RFP and GFP variants), fused to functional modules. These include fluorescent sensors for visualization of Ca^{2+}, H^{+} and ATP/ADP dynamics; oligomerizing or heterodimerizing modules that allow recruitment or sequestration of proteins and identification of membrane contact sites between organelles; SNAP tags that allow labelling with fluorescent dyes and targeted chromophore-assisted light inactivation; and nanobodies targeted to lumenal sub-compartments of the secretory pathway. We also developed two methods for crosslinking tagged proteins: a dimeric nanobody, and RFP-targeting and GFP-targeting nanobodies fused to complementary hetero-dimerizing domains. We show various applications of the toolkit and demonstrate, for example, that IP_3 receptors deliver Ca^{2+} to the outer membrane of only a subset of mitochondria, and that only one or two sites on a mitochondrion form membrane contacts with the plasma membrane.

Conclusions: This toolkit greatly expands the utility of intrabodies for studying cell signalling in live cells.

Background

Visualizing the location of specific proteins within cells and manipulating their function is crucial for understanding cell biology. Antibodies can define protein locations in fixed and permeabilized cells, but antibodies are large protein complexes that are difficult to introduce into live cells [1]. This limits their ability to interrogate the dynamics or affect the function of proteins in live cells. Small protein-based binders, including nanobodies derived from the variable region of the heavy chains (V_{HH}) of camelid antibodies, offer a promising alternative [2]. Nanobodies can be encoded by plasmids and expressed in live cells. However, generating nanobodies against thousands of protein variants is daunting, and even for single targets it can be time-consuming, costly and not always successful. A solution to this bottleneck is provided by fluorescently tagged proteins, which are widely used in cell biology [3, 4] after heterologous expression of proteins or gene editing of endogenous proteins [5-7]. The most common application of fluorescent protein (FP) tags is to visualize protein locations, but they have additional potential as generic affinity tags to manipulate and visualize protein functions in live cells. These opportunities are under-developed.

Green fluorescent protein (GFP) has undergone numerous cycles of optimization as a reporter and non-perturbing tag [3, 8]. Most GFP-tagged proteins therefore retain their endogenous localization and function [9]. Large libraries of plasmids encoding GFP-tagged proteins are now available [10]. Proteome-scale expression of GFP-tagged proteins or genome-scale tagging of gene products with GFP has been reported for *Drosophila* [11], fungi [12-14], plants [15, 16] and bacteria [17].

Proteins tagged with red fluorescent proteins (RFPs) such as DsRed, mRFP and mCherry (mCh) are also popular. Extensive optimization has made them attractive tags [3, 18], and libraries of RFP-tagged proteins have been developed in mouse stem cells [19] and yeast [14].

Nanobodies that bind to RFP [20, 21] or GFP [21, 22] are most commonly used in their purified forms for immunoprecipitation and immunocytochemistry. However, they also offer a generic means of targeting in live cells the huge variety of available tagged proteins and the many emerging examples of endogenous proteins tagged with FPs by gene editing. GFP-targeting nanobodies have been used for applications such as targeted proteosomal degradation [23, 24] and relocation of proteins in cells [25], but these and other applications are less developed for RFP-targeting nanobodies.

Here we develop a plasmid-encoded toolkit of nanobodies that bind common FP tags, including RFPs, CFP, GFP and YFP, fused to functional modules for visualization and manipulation of cell signalling (***Fig. 1***). We fused the nanobodies to a variety of functional modules: fluorescent sensors for Ca^{2+}, H^+ and ATP/ADP; optimized SNAP tags for labelling with bright and photostable dyes [26]; and hetero-dimerizing partners that allow inducible recruitment or sequestration of proteins and visualization of membrane contact sites (MCS) between organelles. We developed two methods to allow crosslinking of RFP-tagged and GFP-tagged proteins: a dimeric nanobody, and co-expression of RFP-targeting and GFP-targeting nanobodies fused to complementary hetero-dimerizing domains. We also describe functionalized nanobodies directed to lumenal sub-compartments of the secretory pathway. We demonstrate the utility of nanobody fusions by visualizing local Ca^{2+} dynamics at the surface of mitochondria, by manipulating the locations of proteins and organelles within cells, by characterizing MCS between mitochondria and the plasma membrane (PM), and by targeting lumenal Ca^{2+} sensors to a sub-compartment of the endoplasmic reticulum (ER).

This versatile toolkit of genetically-encoded, functionalized nanobodies greatly expands the utility of RFP- and GFP-targeting nanobodies. It will provide a valuable resource for studying protein function and cell signalling in live cells. We illustrate some applications and demonstrate, for example, that IP_3 receptors deliver Ca^{2+} to the outer membrane of only some

mitochondria and that MCS between mitochondria and the plasma membrane occur at only one or two sites on each mitochondrion.

Results

Targeting RFP and GFP variants with genetically-encoded nanobody fusions in live cells

The RFP nanobody (RNab) and GFP nanobody (GNab) used are the previously described llama variants LaM4 and LaG16, respectively [21]. They were chosen for their favourable combinations of high affinity (K_d values of 0.18 nM and 0.69 nM, respectively) and ability to bind a variety of RFP or GFP variants [21]. The latter attribute maximizes their potential for targeting a wide variety of FPs [3, 4]. LaM4 binds both mCh and DsRed variants, but not GFPs [21]. In addition to binding GFP, LaG16 binds cyan, blue and yellow FPs (CFP, BFP and YFP), but not RFPs [21]. In contrast, the widely used VhhGFP4 nanobody binds GFP, but not CFP [22].

In HeLa cells with organelles (ER, mitochondria, nucleus and lysosomes) labelled with mCh or mRFP markers, expression of RNab-GFP (***Fig. 2A***) specifically identified the labelled organelle (***Fig. 2B***). Similar results were obtained with GNab-mCh (***Fig. 2C***) and organelles (ER, mitochondria and nucleus) labelled with GFP or mTurquoise (***Fig. 2D***). These results demonstrate that plasmid-encoded RNab and GNab allow specific labelling of a variety of RFP and GFP variants in live cells.

Targeting sensors to RFP and GFP

The effects of intracellular messengers such as Ca^{2+} [27], H^+ [28] and ATP/ADP [29] can be highly localized within cells. To enable visualization of these intracellular messengers in

microdomains around RFP-tagged and GFP-tagged proteins, we fused RNab and GNab to fluorescent sensors for Ca^{2+} [30], H^+ [31, 32] or ATP/ADP [33].

RNab was fused to the green fluorescent Ca^{2+} sensor G-GECO1.2 (***Fig. 3***), and GNab was fused to the red fluorescent Ca^{2+} sensors, R-GECO1.2 or LAR-GECO1.2 [30] (***Fig. 4***). The affinities of these sensors for Ca^{2+} (K_D^{Ca} of 1.2 µM for G-GECO1.2 and R-GECO1.2, and 10 µM for LAR-GECO1.2) are low relative to global changes in the cytosolic free Ca^{2+} concentration ($[Ca^{2+}]_c$) after receptor stimulation (typically ~300 nM) [34]. This facilitates selective detection of the large, local rises in $[Ca^{2+}]$ that are important for intracellular signalling, at the contacts between active inositol 1,4,5-trisphosphate receptors (IP_3Rs) and mitochondria, for example [27]. To allow targeted measurement of relatively low resting $[Ca^{2+}]$ within cellular microdomains we also fused RNab to the ratiometric Ca^{2+}-sensor, GEM-GECO1 (K_D^{Ca} = 300 nM) [30], to give RNab-GEMGECO1 (***Additional file 1: Fig. S1***).

In HeLa cells expressing TOM20-mCh or TOM20-GFP to identify the outer mitochondrial membrane (OMM), the RNab-Ca^{2+} sensors (***Fig. 3*** and ***Additional file 1: Fig. S1***) and GNab-Ca^{2+} sensors (***Fig. 4***) were targeted to the OMM. Both families of targeted sensor reported an increase in $[Ca^{2+}]$ after treatment with the Ca^{2+} ionophore, ionomycin (***Fig. 3, Fig. 4*** and ***Additional file 1: Fig. S1***). This confirms the ability of the sensors to report $[Ca^{2+}]$ changes when targeted to the OMM microdomain.

In some cells, the targeted Nab-Ca^{2+} sensors revealed local changes in $[Ca^{2+}]_c$ after receptor stimulation with histamine, which stimulates IP_3 formation and Ca^{2+} release from the ER in HeLa cells [34]. Imperfect targeting of the RNab-GGECO1.2 to the OMM allowed Ca^{2+} signals at the surface of individual mitochondria to be distinguished from those in nearby cytosol in some cells (***Fig. 3D-F*** and ***Additional file 2: Video 1***). In the example shown, RNab-GGECO1.2 at both the OMM and nearby cytosol responded to the large, global increases in $[Ca^{2+}]$ evoked by ionomycin. However, cytosolic RNab-GGECO1.2 did not

respond to histamine, while the sensor at the OMM responded with repetitive spiking (***Fig. 3D-F*** and ***Additional file 2: Video 1***). The GNab-LARGECO1.2 sensor, which has the lowest affinity for Ca^{2+} of the sensors used, revealed changes in $[Ca^{2+}]_c$ at the surface of some mitochondria, but not others in the same cell (***Fig. 4D-F***, ***Fig. 4H*** and ***Additional file 3: Video 2***). In the example shown, GNab-LARGECO1.2 at the OMM in all mitochondria within the cell responded to the large, global increases in $[Ca^{2+}]$ evoked by ionomycin. However, in response to histamine mitochondria in the perinuclear region responded, but not those in peripheral regions (***Fig. 4D-F***, ***Fig. 4H*** and ***Additional file 3: Video 2***). Ca^{2+} uptake by mitochondria affects many cellular responses, including mitochondrial metabolism, ATP production and apoptosis [35], and Ca^{2+} at the cytosolic face of the OMM regulates mitochondrial motility [36]. The subcellular heterogeneity of mitochondrial exposure to increased $[Ca^{2+}]$ suggests that these reponses may be very localized in cells.

These observations align with previous reports showing that Ca^{2+}-mobilizing receptors evoke both oscillatory $[Ca^{2+}]$ changes within the mitochondrial matrix [37], and large local increases in $[Ca^{2+}]$ at the cytosolic face of the OMM [38]. Our results establish that nanobody-Ca^{2+}-sensor fusions are functional and appropriately targeted, and can be used to detect physiological changes in $[Ca^{2+}]$ within cellular microdomains such as the OMM.

For targeted measurements of intracellular pH, RNab was fused to the green fluorescent pH sensor super-ecliptic pHluorin (SEpHluorin) [31] and GNab was fused to the red fluorescent pH sensor pHuji [32]. Both Nab-pH sensors were targeted to the OMM by the appropriate fluorescent tags, where they responded to changes in intracellular pH imposed by altering extracellular pH in the presence of the H^+/K^+ ionophore nigericin (***Fig. 5***).

For targeted measurements of ATP/ADP, RNab was fused to the excitation-ratiometric ATP/ADP sensor Perceval-HR [33]. RNab-Perceval-HR was targeted to the surface of

mitochondria and responded to inhibition of glycolysis and oxidative phosphorylation (***Fig. 6***).

The results demonstrate that nanobodies can be used to direct sensors for Ca^{2+}, H^{+} or ATP/ADP to specific subcellular compartments tagged with variants of RFP or GFP.

Targeting SNAPf tags to RFP and GFP in live cells

SNAP, and related tags, are versatile because a range of SNAP substrates, including some that are membrane-permeant, can be used to attach different fluorophores or cargoes to the tag [39]. Purified GFP-targeting nanobodies fused to a SNAP tag have been used to label fixed cells for optically demanding applications [40]. We extended this strategy to live cells using RNab and GNab fused to the optimized SNAPf tag [41] (***Fig. 7A*** and ***B***). In cells expressing the mitochondrial marker TOM20-mCh, RNab-SNAPf enabled labelling of mitochondria with the cell-permeable substrate SNAP-Cell 647-SiR and imaging at far-red wavelengths (***Fig. 7C***). In cells expressing lysosomal LAMP1-mCh and RNab-SNAPf, SNAP-Cell 647-SiR instead labelled lysosomes (***Fig. 7D***), demonstrating that SNAP-Cell 647-SiR specifically labelled the organelles targeted by RNab-SNAPf. Similar targeting of SNAP-Cell 647-SiR to mitochondria (***Fig. 7E***) and lysosomes (***Fig. 7F***) was achieved by GNab-SNAPf co-expressed with the appropriate GFP-tagged organelle markers.

Chromophore-assisted light inactivation (CALI) can inactivate proteins or organelles by exciting fluorophores attached to them that locally generate damaging reactive superoxide. Historically, antibodies were used to direct a photosensitizer to its target, but fusion of fluorescent proteins or SNAP tags to proteins of interest is now widely used [42]. RNab-SNAPf and GNab-SNAPf make the SNAP strategy more broadly applicable to CALI applications. We demonstrate this by targeting CALI to the outer surface of lysosomes. We anticipated that CALI in this microdomain might, amongst other effects, disrupt the motility

of lysosomes, which depends on their association with molecular motors [43]. RNab-SNAPf enabled labelling of lysosomes with the CALI probe fluorescein, using the cell-permeable substrate, SNAP-Cell-fluorescein (***Fig. 8A*** and ***B***). Exposure to blue light then immobilized the lysosomes (***Fig. 8C-F*** and ***Additional file 4: Video 3***), indicating a loss of motor-driven motility. Control experiments demonstrated that labelling cytosolic SNAPf with SNAP-Cell-fluorescein (***Additional file 1: Fig. S2A*** and ***S2B***) had significantly less effect on lysosomal motility after exposure to blue light (***Fig. 8F*** and ***Additional file 1: Fig. S2C-E***). These results demonstrate that nanobody-SNAPf fusions allow targeting of fluorescent dyes in live cells, which can be used for re-colouring of tagged proteins or targeted CALI.

Sequestration of proteins tagged with RFP or GFP

Fusion of GFP nanobodies to degrons allows proteosomal degradation of GFP-tagged proteins [24], but the method is slow and cumbersome to reverse. An alternative strategy is to sequester tagged proteins so they cannot fulfil their normal functions. We used two strategies to achieve this: artificial clustering and recruitment to mitochondria.

We induced artificial clustering by fusing RNab or GNab to a multimerizing protein (MP) comprising a dodecameric fragment of Ca^{2+}-calmodulin-dependent protein kinase II (CaMKII) [44], with an intervening fluorescent protein (mRFP or mCerulean) for visualization of the Nab fusion (***Fig. 9A*** and ***B***). RNab-mCerulean-MP caused clustering of the ER transmembrane protein mCh-Sec61β (***Fig. 9C*** and ***D***) and caused lysosomes tagged with LAMP1-mCh to aggregate into abnormally large structures (***Fig. 9E*** and ***F***). GNab-mRFP-MP had the same clustering effect on lysosomes labelled with LAMP1-GFP (***Fig. 9G*** and ***H***) and caused clustering of GFP-tagged proteins in the cytosol (calmodulin, ***Fig. 9I*** and ***J***), nucleus and cytosol (p53, ***Fig. 9K*** and ***L***) or ER membranes (IP_3R3, ***Fig. 9M*** and ***N***).

For inducible sequestration, sometimes known as 'knocksideways' [45], we used two approaches based on hetero-dimerizing modules, one chemical and one optical. First, we adapted the original knocksideways method, where proteins tagged with FKBP (FK506-binding protein) are recruited by rapamycin to proteins tagged with FRB (FKBP-rapamycin-binding domain) on the OMM, and thereby sequestered. The method has hitherto relied on individual proteins of interest being tagged with FKBP [45]. RNab-FKBP and GNab-FKBP (***Fig. 10A*** and ***B***) extend the method to any protein tagged with RFP or GFP. For our analyses, we expressed TOM70 (an OMM protein) linked to FRB through an intermediary fluorescent protein (GFP or mCh, to allow optical identification of the fusion protein). RNab-FKBP sequestered the ER transmembrane protein mCh-Sec61β at the OMM (TOM70-GFP-FRB) within seconds of adding rapamycin (***Additional file 5: Video 4***) and rapidly depleted mCh-Sec61β from the rest of the ER (***Fig. 10C-E***). After addition of rapamycin, GNab-FKBP rapidly sequestered endogenous IP_3R1 tagged with GFP (GFP-IP_3R1) [7] (***Fig. 10F*** and ***G,*** and ***Additional file 6: Video 5***) and cytosolic GFP-tagged calmodulin (***Fig. 10H*** and ***Additional file 7: Video 6***) at mitochondria expressing TOM70-mCh-FRB. Rapamycin caused no sequestration in the absence of the nanobody fusions (***Additional file 1: Fig. S3***).

To make sequestration reversible and optically activated, we adapted the light-oxygen-voltage-sensing domain (LOV2)/Zdark (zdk1) system in which light induces dissociation of LOV2-zdk1 hetero-dimers [46]. Because this system is operated by blue light at intensities lower than required for imaging GFP [46], it is most suitable for use with red fluorescent tags. RNab-zdk1 (***Fig. 11A***) sequestered cytosolic mCh on the OMM in cells expressing TOM20-LOV2, and blue laser light rapidly and reversibly redistributed mCh to the cytosol (***Fig. 11B*** and ***C***).

Inducible recruitment of tagged proteins to membrane contact sites

The ability of Nab-FKBP fusions to recruit membrane proteins to FRB-tagged targets suggested an additional application: revealing contact sites between membrane-bound organelles. ER-mitochondrial membrane contact sites (MCS) have been much studied [47], but contacts between the PM and mitochondria, which are less extensive [48], have received less attention. In HeLa cells co-expressing the PM β_2-adrenoceptor tagged with mCh (β_2AR-mCh), TOM20-GFP-FRB and RNab-FKBP, rapamycin caused rapid recruitment of β_2AR-mCh within the PM to mitochondria at discrete puncta that grew larger with time (***Fig. 12A-E*** and ***Additional file 8: Video 7***). Recruitment was not seen in the absence of co-expressed RNab-FKBP (***Fig. 12F***). Rapamycin also triggered similar punctate accumulation of β_2AR at mitochondria in COS-7 cells expressing β_2AR-GFP, TOM20-mCh-FRB and GNab-FKBP (***Additional file 1: Fig. S4***). In similar analyses of ER-mitochondria and PM-mitochondria MCS, the initial punctate colocalization of proteins was shown to report native MCS, which grew larger with time as rapamycin zipped the proteins together [48]. Our results are consistent with that interpretation. In most cases, β_2AR were recruited to only one or two discrete sites on each mitochondrion, which expanded during prolonged incubation with rapamycin, but without the appearance of new sites (***Fig. 12D*** and **E,** and ***Additional file 1: Fig. S4***). Rapamycin had no evident effect on recruiting new mitochondria to the PM, but it did cause accumulation of tagged TOM70 at MCS and depletion of TOM70 from the rest of each mitochondrion, indicating mobility of TOM70 within the OMM (***Additional file 1: Fig. S4***). Our results suggest that inducible cross-linking using RNab-FKBP or GNab-FKBP identifies native MCS between mitochondria and PM, with each mitochondrion forming only one or two MCS with the PM. We have not explored the functional consequences of these restricted MCS, but we speculate that they may identify sites where proteins involved in communication between the PM and mitochondria are concentrated, facilitating, for example,

phospholipid transfer [49], the generation of ATP microdomains [50], or Ca^{2+} exchanges between mitochondria and store-operated Ca^{2+} entry (SOCE) [51] or PM Ca^{2+}-ATPases [52].

We next tested whether PM proteins could be recruited to the MCS between ER-PM that are important for SOCE and lipid transfer [53]. In response to rapamycin, mCh-Orai1, the PM Ca^{2+} channel that mediates SOCE [54], was recruited by RNab-FKBP to ER-PM MCS labelled with the marker GFP-MAPPER-FRB [55] (***Fig. 13A*** and ***B***). Recruitment was not observed in the absence of RNab-FKBP (***Fig. 13C***). We conclude that the method identifies native ER-PM MCS during the initial phase of Nab recruitment, and the Nab subsequently exaggerates these MCS.

One of the least explored MCS is that between lysosomes and mitochondria [56]. Recent evidence shows that these MCS control the morphology of both organelles [57] and probably mediate exchange of cholesterol and other metabolites between them [58]. We assessed whether the nanobody fusions could be used to inducibly recruit lysosomes to mitochondria. GNab-FKBP enabled recruitment of lysosomes labelled with LAMP1-GFP to mitochondria labelled with TOM20-mCh-FRB, in response to rapamycin (***Fig. 14A-C***). Lysosomes were not recruited to mitochondria in the absence of GNab-FKBP (***Fig. 14D***).

Cross-linking RFP-tagged and GFP-tagged proteins

We generated a dimeric nanobody (GNab-RNab) that binds simultaneously to GFP and RFP (***Fig. 15A***), and demonstrated its utility by crosslinking a variety of GFP-tagged and RFP-tagged proteins. Cytosolic GFP, normally diffusely distributed in the cytosol (data not shown), was recruited to nuclei by H2B-mCh (***Fig. 15B***) or to mitochondria by TOM20-mCh (***Fig. 15C***). In the presence of GNab-RNab, mCh-Orai1 and endogenously tagged GFP-IP_3R1 formed large co-clusters (***Fig 15D***) that differed markedly from the distributions of GFP-IP_3R1 (***Fig. 10F***) and mCh-Orai1 (***Fig 13***) in the absence of crosslinking. Consistent

with earlier results (***Fig. 12*** and ***Additional file 1: Fig. S4***), β_2AR-mCh, which is normally diffusely distributed in the PM, formed mitochondria-associated puncta when crosslinked to mitochondria expressing TOM20-GFP (***Fig. 15E***). Whole organelles could also be crosslinked. Co-expression of LAMP1-GFP and LAMP1-mCh labelled small, mobile lysosomes in control cells (***Fig. 15F***), while additional co-expression of GNab-RNab caused accumulation of lysosomes into large clusters (***Fig. 15G***).

This crosslinking of GFP and RFP was made rapidly inducible with an RNab-FRB fusion that hetero-dimerizes with GNab-FKBP in the presence of rapamycin (***Fig. 16A***). Co-expression of GNab-FKBP with RNab-FRB in cells co-expressing TOM20-GFP and mCh-Sec61β led to rapid colocalization of GFP and mCh after addition of rapamycin (***Fig. 16B*** and ***C,*** and ***Additional file 9: Video 8***). Similar results were obtained with RNab-FKBP and GNab-FRB (***Additional file 1: Fig. S5***). We conclude that GNab-FKBP and RNab-FRB provide a rapidly inducible system for crosslinking any GFP-tagged protein to any RFP-tagged protein.

Targeting secretory compartments with lumenal nanobodies

GNab and RNab were directed to the lumen of the secretory pathway by addition of an N-terminal signal sequence, giving ssGNab and ssRNab. Targeting of ssGNab-mCh to the Golgi, ER network,or ER-PM MCS was achieved by co-expression of organelle markers with lumenal FP tags (***Fig. 17A*** and ***B***). In each case, there was significant colocalization of green and red proteins. Similar targeting of ssRNab-GFP to the ER network or ER-PM MCS was achieved by co-expression with mCh-tagged lumenal markers of these organelles (***Fig. 17C*** and ***D***). These results demonstrate that ssGNab and ssRNab fusions can be directed to the lumen of specific compartments of the secretory pathway.

Fluorescent Ca^{2+} sensors targeted to the lumen of the entire ER [59, 60] are widely used and have considerably advanced our understanding of Ca^{2+} signalling [61, 62]. Fluorescent Ca^{2+} sensors targeted to ER sub-compartments and the secretory pathway have received less attention but have, for example, been described for the Golgi [63, 64]. Our nanobody methods suggest a generic approach for selective targeting of lumenal Ca^{2+} indicators. Fusion of ssRNab to GCEPIA1 or GEM-CEPIA [60] provided ssRNab-GCEPIA1 and ssRNab-GEMCEPIA (***Fig. 18A***). These fusions were targeted to the lumenal aspect of ER-PM junctions by co-expression with mCh-MAPPER [7] (***Fig. 18C*** and ***D***). Fusion of ssGNab to the low-affinity Ca^{2+} sensors LAR-GECO1 [59] or RCEPIA1 [60] provided ssGNab-LARGECO1 and ssGNab-RCEPIA1 (***Fig. 18B***). These fusions allowed targeting to ER-PM junctions labelled with GFP-MAPPER (***Fig. 18E*** and ***F***). The targeted Ca^{2+} sensors responded appropriately to emptying of intracellular Ca^{2+} stores by addition of ionomycin in Ca^{2+}-free medium (***Fig. 18G-K***). These results confirm that Ca^{2+} sensors targeted to a physiologically important ER sub-compartment, the ER-PM junctions where SOCE occurs, report changes in lumenal [Ca^{2+}]. Our results demonstrate that nanobody fusions can be targeted to lumenal sub-compartments of the secretory pathway and they can report [Ca^{2+}] within physiologically important components of the ER.

Discussion

The spatial organization of the cell interior influences all cellular activities and it is a recurrent theme in intracellular signalling [65, 66]. Hence, tools that can visualize and manipulate the spatial organization of intracellular components are likely to find widespread application. We introduce a toolkit of plasmids encoding functionalized nanobodies against common FP tags, including CFP, GFP, YFP and RFPs (***Fig. 1***). Use of this toolkit is supported by genome-wide collections of plasmids, cells and organisms expressing proteins

tagged with GFP and RFP [10-17, 19], and by facile methods for heterologous expression of tagged proteins or editing of endogenous genes to encode FP tags [5, 6]. The functionalized nanobodies provide new approaches to studying intracellular signalling in live cells.

Our toolkit expands the repertoire of functionalized RFP-binding nanobodies, which are less developed than their GFP-binding counterparts [67]. The RNab fusions provide new opportunities to use RFP, which often has advantages over GFP. For example, RFP is spectrally independent from blue-green sensors, which are usually superior to their red counterparts [30, 32]; from the CALI probe, fluorescein; and from optogenetic modules, which are often operated by blue-green light [68].

Nanobody-sensor fusions allow targeting of sensors to specific proteins and organelles (***Figs. 2-6***), and will aid visualization of signalling within cellular microdomains. Fusion of nanobodies to the Ca^{2+} sensors G-GECO1.2, R-GECO1.2 and LAR-GECO1.2 [30] (***Figs. 3*** and ***4***), which have relatively low affinities for Ca^{2+} (K_D values of 1.2 µM, 1.2 µM and 10 µM, respectively), should facilitate selective detection of the relatively large, local rises in $[Ca^{2+}]_c$ that are important for cell signalling [27]. The GEM-GECO Ca^{2+} sensor [30], H^+ sensors [31, 32] and ATP/ADP sensors [33] used for nanobody fusions are poised to detect fluctuations of their ligands around resting concentrations in the cell (***Figs. 4-6***).

Relative to direct fusions of sensors to proteins of interest, nanobody-sensor fusions have several advantages. Firstly, the generic nanobody toolkit (***Fig. 1***) can be combined with collections of FP-tagged proteins to provide many combinations; each would otherwise require expression of a unique construct. Secondly, each sensor is attached to the same entity (nanobody), which binds to the same partner (FP). Since the biophysical and biochemical properties of sensors may be influenced by their fusion partners, this provides greater confidence that sensors despatched to different locations will respond similarly to their analyte.

Nanobodies allow re-colouring of FPs. Nanobody-SNAPf fusions, for example, can be used to attach fluorescent dyes, including CALI probes and far-red fluorophores, to FP tags (***Figs. 7*** and ***8***). Longer excitation wavelengths cause less phototoxicity and allow greater penetration through tissue, which may be useful in studies of transgenic organisms and tissues. We also envisage live-cell applications in pulse-chase analyses and using super-resolution microscopy, Förster resonance energy transfer (FRET) and fluorescence lifetime imaging.

Membrane-permeant forms of the SNAP ligand, O^6-benzylguanine, are available conjugated to conventional Ca^{2+} indicators (Fura-2FF, Indo-1 and BOCA-1), which are brighter than genetically-encoded indicators [69-71]; to derivatives of the two-photon fluorophore naphthalimide [72]; to the hydrogen peroxide sensor nitrobenzoylcarbonylfluorescein [73]; and to reversible chemical dimerizers [74, 75]. Nanobody-SNAPf fusions will allow facile targeting of these modules to any protein or organelle tagged with RFP or GFP.

Cross-linking methods have many applications in cell biology, including stabilizing protein interactions (eg, for pull-downs), identifying and manipulating MCS, enforcing protein interactions (eg, receptor dimerization), redirecting proteins to different subcellular locations (eg, knocksideways) and many more. Functionalized nanobodies provide many additional opportunities to regulate protein associations. The nanobody-FKBP/FRB fusions, for example, allow rapid rapamycin-mediated crosslinking of any pair of proteins tagged with GFP/RFP, or tagged with either FP and any of the many proteins already tagged with FKBP or FRB [76] (***Figs. 10*** and ***12-16***). Nanobody-FKBP fusions may allow crosslinking to SNAP-tagged proteins [75], and the nanobody-SNAPf fusions to HaloTag-tagged proteins [74] and FKBP-tagged proteins [75]. RNab-zdk1 fusions allow photo-inducible crosslinking of RFP-tagged proteins to LOV-tagged proteins [46] (***Fig. 11***). Nanobodies that crosslink

GFP-tagged proteins to RFP-tagged proteins (GNab-RNab; and the GNab-FKBP/RNab-FRB and GNab-FRB/RNab-FKBP pairings) may have the most applications, as they can take fullest advantage of the numerous combinations of existing RFP and GFP-tagged proteins (***Figs. 15*** and ***16***) .

Functionalized nanobodies directed to lumenal compartments of the secretory pathway would provide useful tools, but they are under-developed. Their potential is shown by nanobodies retained within the ER, which restrict onward trafficking of target proteins and inhibit their function [77]. We show that functionalized nanobodies, including nanobody-Ca^{2+} sensors, can be directed to sub-compartments of the secretory pathway (***Figs. 17*** and ***18***). Lumenal Ca^{2+} provides a reservoir within the ER, Golgi and lysosomes that can be released by physiological stimuli to generate cytosolic Ca^{2+} signals [78, 79]. Compartmentalization of Ca^{2+} stores within the ER [63] and Golgi [79] adds to the complexity of lumenal Ca^{2+} distribution in cells. Furthermore, lumenal Ca^{2+} itself regulates diverse aspects of cell biology, including SOCE [54], sorting of cargo in the Golgi [80], binding of ERGIC-53 to cargoes within the ER-Golgi intermediate compartment (ERGIC) [81], and exocytosis of neurotransmitters by secretory vesicles [82, 83]. Hence, there is a need for tools that can effectively report lumenal [Ca^{2+}] within this complex lumenal environment. The lumenal nanobody-Ca^{2+} sensors detected changes in lumenal [Ca^{2+}] at the ER-PM MCS where SOCE occurs (***Fig. 18***).

In addition to nanobodies, other protein-based binders, including single-domain antibodies, designed ankyrin-repeat proteins (DARPINs), affimers, anticalins, affibodies and monobodies have been developed to recognise many important intracellular proteins [2, 84-86]. These binding proteins can be easily transplanted into the fusion scaffolds described to maximize their exploitation.

Conclusions

We present a toolkit of plasmids encoding functionalized nanobodies directed against common fluorescent protein tags, which will allow a wide range of applications and new approaches to studying intracellular signalling in live cells. We illustrate some applications and demonstrate, for example, that IP_3 receptors deliver Ca^{2+} to the OMM of only some mitochondria, and that MCS between mitochondria and the plasma membrane occur at only one or two sites on each mitochondrion.

Materials and Methods

Materials

Human fibronectin was from Merck Millipore. Ionomycin was from Apollo Scientific (Stockport, UK). Rapamycin was from Cambridge Bioscience (Cambridge, UK). SNAP substrates were from New England Biolabs (Hitchin, UK). Other reagents, including histamine and nigericin, were from Sigma-Aldrich.

Plasmids

Sources of plasmids encoding the following proteins were: mCherry-C1 (Clontech #632524); GFP-ERcyt, mCherry-ERcyt and mTurquoise2-ERcyt (GFP, mCherry or mTurquoise2 targeted to the cytosolic side of the ER membrane via the ER-targeting sequence of the yeast UBC6 protein) [87]; mCherry-ERlumen (Addgene #55041, provided by Michael Davidson); LAMP1-mCherry [88]; TPC2-mRFP [89]; TOM20-mCherry (Addgene #55146, provided by Michael Davidson); CIB1-mRFP-MP (Addgene #58367) [44]; CIB1-mCerulean-MP (Addgene #58366) [44]; H2B-GFP (Addgene #11680) [90]; TOM20-LOV2 (Addgene #81009) [46]; mCherry-Sec61β [91]; GFP-MAPPER [55]; GFP-

CaM (Addgene #47602, provided by Emanuel Strehler); TOM70-mCherry-FRB (pMito-mCherry-FRB, Addgene #59352) [92]; pmTurquoise2-Golgi (Addgene #36205) [93]; pTriEx-mCherry-zdk1 (Addgene #81057) [46]; pTriEx-NTOM20-LOV2 (Addgene #81009) [46]; β_2AR-mCFP (Addgene #38260) [94]; pCMV-G-CEPIA1er (Addgene #58215) [60]; pCMV-R-CEPIA1er (Addgene #58216) [60]; pCIS-GEM-CEPIA1er (Addgene #58217) [60]; CMV-ER-LAR-GECO1 and CMV-mito-LAR-GECO1.2 [59]; mCherry-MAPPER and mCherry-Orai1 [7].

H2B-mCh was made by transferring H2B from H2B-GFP to pmCherry-N1 (Clontech) using *Kpn*I/*Bam*HI. LAMP1-GFP was made by transferring LAMP1 from LAMP1-mCherry into pEGFP-N1 (Clontech) using *Eco*RI/*Bam*HI. β_2AR-mCherry was made by transferring β_2AR from β_2AR-mCFP to pmCherry-N1 (Clontech) using *Nhe*I/*Xho*I. β_2AR-GFP was made by transferring GFP from pEGFP-N1 (Clontech) into β_2AR-mCherry using *Xho*I/*Not*I. The mCherry-Golgi plasmid was made by transferring mCherry from pmCherry-N1 into pEYFP-Golgi (Clontech) using *Age*I/*Not*I. GFP-Golgi was made by transferring GFP from pEGFP-N1 (Clontech) into Golgi-mCherry using *Age*I/*Not*I. TOM20-GFP was made by transferring EGFP from pEGFP-N1 into TOM20-mCherry using *Bam*HI/*Not*I. TOM70-GFP-FRB was made by insertion of EGFP from pEGFP-N1 into TOM70-mCh-FRB using *Age*I/*Bsr*GI. SNAPf-pcDNA3.1(+) was made by transferring SNAPf from pSNAPf (New England Biolabs) to pcDNA3.1 (+) using *Nhe*I/*Not*I.

DNA constructs encoding GNab and RNab were synthesized as DNA Strings (ThermoFisher) and introduced by Gibson assembly (Gibson Assembly Master Mix, New England Biolabs) into pcDNA3.1(+) digested with *Bam*HI/*Eco*RI. Sequences encoding GNab and RNab are shown in ***Additional file 1: Fig. S6.*** Plasmids encoding nanobody fusion constructs (***Fig. 1***) were constructed from the GNab and RNab plasmids using PCR,

restriction digestion and ligation, or synthetic DNA Strings and Gibson assembly, and their sequences were confirmed.

RNab-mCerulean-MP was made by PCR of RNab using forward (ATGCTAGCAAGCTTGCCACCATGGCTC) and reverse (ATACCGGTGAGGATCCAGAGCCTCCGC) primers, followed by insertion into CIB1-mCerulean-MP using *Nhe*I/*Age*I. GNab-mRFP-MP was made by PCR of GNab-FKBP with forward (TAGCTAGCGCCACCATGGCTCAGGTG) and reverse (CGACCGGTACGGACACGGTCACTTGGG) primers, and insertion into CIB1-mRFP1-MP using *Nhe*I/*Age*I. RNab-mCerulean-MP was made by PCR of RNab-pcDNA3.1 (+) using forward (ATGCTAGCAAGCTTGCCACCATGGCTC) and reverse (GCGGAGGCTCTGGATCCTCACCGGTAT) primers, followed by transfer into CIB1-mCerulean-MP using *Nhe*I/*Age*I. GNab-SNAPf and RNab-SNAPf were made by PCR of GNab-pcDNA3.1(+) and RNab-pCDNA3.1(+) using forward (CAGCTAGCTTGGTACCGAGCTCAAGCTTGC) and reverse (ATGAATTCAGATCCCCCTCCGCCAC) primers, followed by insertion into SNAPf-pcDNA3.1 (+) using *Nhe*I/*Eco*RI.

ss-GNab-mCherry was made by inserting mCherry from GNab-mCherry into ss-GNab-FKBP using *Bam*HI/*Not*I. ss-RNab-GFP was made by inserting GFP from RNab-GFP into ss-RNab-pcDNA3.1(+) using *Bam*HI/*Not*I. ss-GNab-RCEPIA was made by transferring RCEPIA from pCMV-R-CEPIA1er to ss-RNab-pcDNA3.1(+) using *Bam*HI/*Not*I. ss-RNab-GCEPIA was made by transferring GCEPIA from pCMV-G-CEPIA1er to ss-RNab-pcDNA3.1(+) using *Bam*HI/*Not*I. ss-RNab-GEMCEPIA was made by transferring GEM-CEPIA from pCIS-GEM-CEPIA1er to ss-RNab-pcDNA3.1(+) using *Bam*HI/*Not*I.

Cell culture and transient transfection

HeLa and COS-7 cells (American Type Culture Collection) were cultured in Dulbecco's modified Eagle's medium/F-12 with GlutaMAX (ThermoFisher) supplemented with foetal bovine serum (FBS, 10%, Sigma). Cells were maintained at 37°C in humidified air with 5% CO_2, and passaged every 3-4 days using Gibco TrypLE Express (ThermoFisher). For imaging, cells were grown on 35-mm glass-bottomed dishes (#P35G-1.0-14-C, MatTek) coated with human fibronectin (10 µg ml^{-1}). Cells were transfected, according to the manufacturer's instructions, using TransIT-LT1 (GeneFlow) (1 µg DNA per 2.5 µl reagent). Short tandem repeat profiling (Eurofins, Germany) was used to authenticate the identity of HeLa cells [7]. Screening confirmed that all cells were free of mycoplasma infection.

Fluorescence microscopy and analysis

Cells were washed prior to imaging at 20°C in HEPES-buffered saline (HBS: NaCl 135 mM, KCl 5.9 mM, $MgCl_2$ 1.2 mM, $CaCl_2$ 1.5 mM, HEPES 11.6 mM, D-glucose 11.5 mM, pH 7.3). Ca^{2+}-free HBS lacked $CaCl_2$ and contained EGTA (1 mM). For manipulations of intracellular pH, cells were imaged in modified HBS (MHBS: KCl 140 mM, $MgCl_2$ 1.2 mM, $CaCl_2$ 1.5 mM, HEPES 11.6 mM, D-glucose 11.5 mM, pH 7.2). The H^+/K^+ ionophore nigericin (10 µM) was added 5 min before imaging to equilibrate intracellular and extracellular pH, and the extracellular pH was then varied during imaging by exchanging the MHBS (pH 6.5 or pH 8).

Fluorescence microscopy was performed at 20°C as described previously [7] using an inverted Olympus IX83 microscope equipped with a 100× oil-immersion TIRF objective (numerical aperture, NA 1.49), a multi-line laser bank (425, 488, 561 and 647 nm) and an iLas2 targeted laser illumination system (Cairn, Faversham, Kent, UK). Excitation light

was transmitted through either a quad dichroic beam splitter (TRF89902-QUAD) or a dichroic mirror (for 425 nm; ZT442rdc-UF2) (Chroma). Emitted light was passed through appropriate filters (Cairn Optospin; peak/bandwidth: 480/40, 525/50, 630/75 and 700/75 nm) and detected with an iXon Ultra 897 electron multiplied charge-coupled device (EMCCD) camera (512 × 512 pixels, Andor). For TIRFM, the penetration depth was 100 nm. The iLas2 illumination system was used for TIRFM and wide-field imaging. For experiments with RNab-PercevalHR, a 150× oil-immersion TIRF objective (NA 1.45) and a Prime 95B Scientific metal-oxide-semiconductor (CMOS) camera (512 × 512 pixels, Photometrics) were used.

For CALI and LOV2/zdk1 experiments, the 488-nm laser in the upright position delivered an output at the objective of 2.45 mW (PM100A power meter, Thor Labs, Newton, NJ, USA). For CALI, a single flash of 488-nm laser illumination (3-s duration) was applied, with 10-ms exposures to 488-nm laser immediately before and after the CALI flash to allow imaging of SNAP-Cell-fluorescein (i.e. 3.02 s total CALI flash). For LOV2/zdk1 experiments, repeated flashes of 488-nm light (1-s duration each) were used at 2-s intervals to allow imaging with 561-nm laser illumination during the intervening periods.

Before analysis, all fluorescence images were corrected for background by subtraction of fluorescence detected from a region outside the cell. Image capture and processing used MetaMorph Microscopy Automation and Image Analysis Software (Molecular Devices) and Fiji [95]. Particle tracking used the TrackMate ImageJ plugin [96], with an estimated blob diameter of 17 pixels and a threshold of 5 pixels. Co-localization analysis used the JACoP ImageJ plugin [97]. Pearson's correlation coefficient (*r*) was used to quantify colocalization. We report *r* values only when the Costes' randomization-based colocalization value (P-value = 100 after 100 iterations) confirmed the significance of the original

colocalization. Where example images are shown, they are representative of at least three independent experiments (individual plates of cells from different transfections and days).

Statistics

Results are presented as mean ± SEM for particle-tracking analyses and mean ± SD for colocalization analyses, from *n* independent analyses (individual plates of cells from different transfections). Statistical comparisons used paired or unpaired Student's *t*-tests, or analysis of variance with the Bonferroni correction used for multiple comparisons. $^{*}p < 0.05$ was considered significant.

Availability of data and materials

All plasmids and data generated or analysed in this study are available from the corresponding author on reasonable request.

Competing interests

The authors confirm that they have no competing interests.

Funding

This work was supported by the Biotechnology and Biological Sciences Research Council UK (grant number BB/P005330/1) and a Wellcome Trust Senior Investigator Award (grant number 101844).

Authors' contributions

DLP and CWT conceived the work. DLP conducted all experiments and analysis. DLP and CWT interpreted data and wrote the manuscript. DLP and CWT approved the final manuscript.

Acknowledgements

Not applicable.

References

1. Clift D, McEwan WA, Labzin LI, Konieczny V, Mogessie B, James LC, et al. A method for the acute and rapid degradation of endogenous proteins. Cell. 2018;171:1692-706.e18.
2. Helma J, Cardoso MC, Muyldermans S, Leonhardt H. Nanobodies and recombinant binders in cell biology. J Cell Biol. 2015;209:633-44.
3. Shaner NC, Steinbach PA, Tsien RY. A guide to choosing fluorescent proteins. Nat Methods. 2005;2:905-9.
4. Rodriguez EA, Campbell RE, Lin JY, Lin MZ, Miyawaki A, Palmer AE, et al. The growing and glowing toolbox of fluorescent and photoactive proteins. Trends Biochem Sci. 2017;42:111-29.
5. Leonetti MD, Sekine S, Kamiyama D, Weissman JS, Huang B. A scalable strategy for high-throughput GFP tagging of endogenous human proteins. Proc Natl Acad Sci USA. 2016;113:E3501-E8.
6. Stewart-Ornstein J, Lahav G. Dynamics of CDKN1A in single cells defined by an endogenous fluorescent tagging toolkit. Cell Rep. 2016;14:1800-11.

588 7. Thillaiappan NB, Chavda AP, Tovey SC, Prole DL, Taylor CW. Ca^{2+} signals initiate at
589 immobile IP_3 receptors adjacent to ER-plasma membrane junctions. Nat Commun.
590 2017;8:1505.
591 8. Zhang J. The colorful journey of green fluorescent protein. ACS Chem Biol. 2009;4:85-
592 8.
593 9. Stadler C, Rexhepaj E, Singan VR, Murphy RF, Pepperkok R, Uhlen M, et al.
594 Immunofluorescence and fluorescent-protein tagging show high correlation for protein
595 localization in mammalian cells. Nat Methods. 2013;10:315-23.
596 10. Hein MY, Hubner NC, Poser I, Cox J, Nagaraj N, Toyoda Y, et al. A human
597 interactome in three quantitative dimensions organized by stoichiometries and
598 abundances. Cell. 2015;163:712-23.
599 11. Nagarkar-Jaiswal S, Lee PT, Campbell ME, Chen K, Anguiano-Zarate S, Gutierrez
600 MC, et al. A library of MiMICs allows tagging of genes and reversible, spatial and
601 temporal knockdown of proteins in Drosophila. eLife. 2015;4:e05338.
602 12. Huh WK, Falvo JV, Gerke LC, Carroll AS, Howson RW, Weissman JS, et al. Global
603 analysis of protein localization in budding yeast. Nature. 2003;425:686-91.
604 13. Hayashi A, Ding DQ, Tsutsumi C, Chikashige Y, Masuda H, Haraguchi T, et al.
605 Localization of gene products using a chromosomally tagged GFP-fusion library in the
606 fission yeast Schizosaccharomyces pombe. Genes Cells. 2009;14:217-25.
607 14. Yofe I, Weill U, Meurer M, Chuartzman S, Zalckvar E, Goldman O, et al. One library
608 to make them all: streamlining the creation of yeast libraries via a SWAp-Tag strategy.
609 Nat Methods. 2016;13:371-8.
610 15. Koroleva OA, Tomlinson ML, Leader D, Shaw P, Doonan JH. High-throughput protein
611 localization in Arabidopsis using Agrobacterium-mediated transient expression of GFP-
612 ORF fusions. Plant J. 2005;41:162-74.

16. Tian GW, Mohanty A, Chary SN, Li S, Paap B, Drakakaki G, et al. High-throughput fluorescent tagging of full-length *Arabidopsis* gene products in planta. Plant Physiol. 2004;135:25-38.

17. Kitagawa M, Ara T, Arifuzzaman M, Ioka-Nakamichi T, Inamoto E, Toyonaga H, et al. Complete set of ORF clones of Escherichia coli ASKA library (a complete set of E. coli K-12 ORF archive): unique resources for biological research. DNA Res. 2005;12:291-9.

18. Eason MG, Damry AM, Chica RA. Structure-guided rational design of red fluorescent proteins: towards designer genetically-encoded fluorophores. Curr Opin Struct Biol. 2017;45:91-9.

19. Harikumar A, Edupuganti RR, Sorek M, Azad GK, Markoulaki S, Sehnalova P, et al. An endogenously tagged fluorescent fusion protein library in mouse embryonic stem cells. Stem Cell Rep. 2017;9:1304-14.

20. Pollithy A, Romer T, Lang C, Muller FD, Helma J, Leonhardt H, et al. Magnetosome expression of functional camelid antibody fragments (nanobodies) in *Magnetospirillum gryphiswaldense*. Appl Environ Microbiol. 2011;77:6165-71.

21. Fridy PC, Li Y, Keegan S, Thompson MK, Nudelman I, Scheid JF, et al. A robust pipeline for rapid production of versatile nanobody repertoires. Nat Methods. 2014;11:1253-60.

22. Rothbauer U, Zolghadr K, Muyldermans S, Schepers A, Cardoso MC, Leonhardt H. A versatile nanotrap for biochemical and functional studies with fluorescent fusion proteins. Mol Cell Proteomics. 2008;7:282-9.

23. Kanner SA, Morgenstern T, Colecraft HM. Sculpting ion channel functional expression with engineered ubiquitin ligases. eLife. 2017;6:e29744.

637 24. Caussinus E, Kanca O, Affolter M. Fluorescent fusion protein knockout mediated by
638 anti-GFP nanobody. Nat Struct Mol Biol. 2011;19:117-21.
639 25. Borg S, Popp F, Hofmann J, Leonhardt H, Rothbauer U, Schuler D. An intracellular
640 nanotrap redirects proteins and organelles in live bacteria. MBio. 2015;6:e02117.
641 26. Liu TK, Hsieh PY, Zhuang YD, Hsia CY, Huang CL, Lai HP, et al. A rapid SNAP-tag
642 fluorogenic probe based on an environment-sensitive fluorophore for no-wash live cell
643 imaging. ACS Chem Biol. 2014;9:2359-65.
644 27. Filadi R, Pozzan T. Generation and functions of second messengers microdomains. Cell
645 Calcium. 2015;58:405-14.
646 28. Ludwig FT, Schwab A, Stock C. The Na^+ /H^+ -exchanger (NHE1) generates pH
647 nanodomains at focal adhesions. J Cell Physiol. 2012;228:1351-8.
648 29. Schlattner U, Klaus A, Ramirez Rios S, Guzun R, Kay L, Tokarska-Schlattner M.
649 Cellular compartmentation of energy metabolism: creatine kinase microcompartments
650 and recruitment of B-type creatine kinase to specific subcellular sites. Amino Acids.
651 2016;48:1751-74.
652 30. Zhao Y, Araki S, Wu J, Teramoto T, Chang YF, Nakano M, et al. An expanded palette
653 of genetically encoded Ca^{2+} indicators. Science. 2011;333:1888-91.
654 31. Sankaranarayanan S, De Angelis D, Rothman JE, Ryan TA. The use of pHluorins for
655 optical measurements of presynaptic activity. Biophys J. 2000;79:2199-208.
656 32. Shen Y, Rosendale M, Campbell RE, Perrais D. pHuji, a pH-sensitive red fluorescent
657 protein for imaging of exo- and endocytosis. J Cell Biol. 2014;207:419-32.
658 33. Tantama M, Martinez-Francois JR, Mongeon R, Yellen G. Imaging energy status in
659 live cells with a fluorescent biosensor of the intracellular ATP-to-ADP ratio. Nat
660 Commun. 2013;4:2550.

661 34. Atakpa P, Thillaiappan NB, Mataragka S, Prole DL, Taylor CW. IP_3 receptors
662 preferentially associate with ER-lysosome contact sites and selectively deliver Ca^{2+} to
663 lysosomes. Cell Rep. 2018;25:3180-93.
664 35. Mammucari C, Raffaello A, Vecellio Reane D, Gherardi G, De Mario A, Rizzuto R.
665 Mitochondrial calcium uptake in organ physiology: from molecular mechanism to
666 animal models. Pflugers Archive. 2018;470:1165-79.
667 36. Wang X, Schwarz TL. The mechanism of Ca^{2+} -dependent regulation of kinesin-
668 mediated mitochondrial motility. Cell. 2009;136:163-74.
669 37. Hajnóczky G, Robb-Gaspers LD, Seitz MB, Thomas AP. Decoding cytosolic calcium
670 oscillations in the mitochondria. Cell. 1995;82:415-24.
671 38. Giacomello M, Drago I, Bortolozzi M, Scorzeto M, Gianelle A, Pizzo P, et al. Ca^{2+} hot
672 spots on the mitochondrial surface are generated by Ca^{2+} mobilization from stores, but
673 not by activation of store-operated Ca^{2+} channels. Mol Cell. 2010;38:280-90.
674 39. Cole NB. Site-specific protein labeling with SNAP-tags. Curr Prot Prot Sci.
675 2014;73:Unit 30.1.
676 40. Ries J, Kaplan C, Platonova E, Eghlidi H, Ewers H. A simple, versatile method for
677 GFP-based super-resolution microscopy via nanobodies. Nat Methods. 2012;9:582-4.
678 41. Bodor DL, Rodriguez MG, Moreno N, Jansen LE. Analysis of protein turnover by
679 quantitative SNAP-based pulse-chase imaging. Curr Prot Cell Biol. 2012:Unit 8.
680 42. Sano Y, Watanabe W, Matsunaga S. Chromophore-assisted laser inactivation - towards
681 a spatiotemporal-functional analysis of proteins, and the ablation of chromatin,
682 organelle and cell function. J Cell Sci. 2014;127:1621-9.
683 43. Bonifacino JS, Neefjes J. Moving and positioning the endolysosomal system. Curr
684 Opin Cell Biol. 2017;47:1-8.

685 44. Lee S, Park H, Kyung T, Kim NY, Kim S, Kim J, et al. Reversible protein inactivation
686 by optogenetic trapping in cells. Nat Methods. 2014;11:633-6.
687 45. Robinson MS, Sahlender DA, Foster SD. Rapid inactivation of proteins by rapamycin-
688 induced rerouting to mitochondria. Dev Cell. 2010;18:324-31.
689 46. Wang H, Vilela M, Winkler A, Tarnawski M, Schlichting I, Yumerefendi H, et al.
690 LOVTRAP: an optogenetic system for photoinduced protein dissociation. Nat Methods.
691 2016;13:755-8.
692 47. Csordas G, Weaver D, Hajnoczky G. Endoplasmic reticular-mitochondrial
693 contactology: structure and signaling functions. Trends Cell Biol. 2018;28:523-40.
694 48. Csordas G, Varnai P, Golenar T, Roy S, Purkins G, Schneider TG, et al. Imaging
695 interorganelle contacts and local calcium dynamics at the ER-mitochondrial interface.
696 Mol Cell. 2010;39:121-32.
697 49. Tepikin AV. Mitochondrial junctions with cellular organelles: Ca^{2+} signalling
698 perspective. Pflugers Archive. 2018;470:1181-92.
699 50. Kennedy HJ, Pouli AE, Ainscow EK, Jouaville LS, Rizzuto R, Rutter GA. Glucose
700 generates sub-plasma membrane ATP microdomains in single islet beta-cells. Potential
701 role for strategically located mitochondria. J Biol Chem. 1999;274:13281-91.
702 51. Quintana A, Pasche M, Junker C, Al-Ansary D, Rieger H, Kummerow C, et al. Calcium
703 microdomains at the immunological synapse: how ORAI channels, mitochondria and
704 calcium pumps generate local calcium signals for efficient T-cell activation. EMBO J.
705 2011;30:3895-912.
706 52. Frieden M, Arnaudeau S, Castelbou C, Demaurex N. Subplasmalemmal mitochondria
707 modulate the activity of plasma membrane Ca^{2+}-ATPases. J Biol Chem.
708 2005;280:43198-208.

709 53. Balla T. Ca^{2+} and lipid signals hold hands at endoplasmic reticulum-plasma membrane
710 contact sites. J Physiol. 2017;596:2709-16.
711 54. Prakriya M, Lewis RS. Store-operated calcium channels. Physiol Rev. 2015;95:1383-
712 436.
713 55. Chang CL, Hsieh TS, Yang TT, Rothberg KG, Azizoglu DB, Volk E, et al. Feedback
714 regulation of receptor-induced Ca^{2+} signaling mediated by E-Syt1 and Nir2 at
715 endoplasmic reticulum-plasma membrane junctions. Cell Rep. 2013;5:813-25.
716 56. Simmen T, Tagaya M. Organelle communication at membrane contact sites (MCS):
717 from curiosity to center stage in cell biology and biomedical research. Adv Exp Med
718 Biol. 2017;997:1-12.
719 57. Wong YC, Ysselstein D, Krainc D. Mitochondria-lysosome contacts regulate
720 mitochondrial fission via RAB7 GTP hydrolysis. Nature. 2017;554:382-6.
721 58. Torres S, Balboa E, Zanlungo S, Enrich C, Garcia-Ruiz C, Fernandez-Checa JC.
722 Lysosomal and mitochondrial liaisons in Niemann-Pick disease. Front Physiol.
723 2017;8:982.
724 59. Wu J, Prole DL, Shen Y, Lin Z, Gnanasekaran A, Liu Y, et al. Red fluorescent
725 genetically encoded Ca^{2+} indicators for use in mitochondria and endoplasmic reticulum.
726 Biochem J. 2014;464:13-22.
727 60. Suzuki J, Kanemaru K, Ishii K, Ohkura M, Okubo Y, Iino M. Imaging intraorganellar
728 Ca^{2+} at subcellular resolution using CEPIA. Nat Commun. 2014;5:4153.
729 61. Suzuki J, Kanemaru K, Iino M. Genetically encoded fluorescent indicators for
730 organellar calcium imaging. Biophys J. 2016;111:1119-31.
731 62. Hirabayashi Y, Kwon SK, Paek H, Pernice WM, Paul MA, Lee J, et al. ER-
732 mitochondria tethering by PDZD8 regulates Ca^{2+} dynamics in mammalian neurons.
733 Science. 2017;358:623-30.

734 63. Konieczny V, Tovey SC, Mataragka S, Prole DL, Taylor CW. Cyclic AMP recruits a
735 discrete intracellular Ca^{2+} store by unmasking hypersensitive IP_3 receptors. Cell Rep.
736 2017;18:711-22.
737 64. Rodriguez-Prados M, Rojo-Ruiz J, Aulestia FJ, Garcia-Sancho J, Alonso MT. A new
738 low-Ca^{2+} affinity GAP indicator to monitor high Ca^{2+} in organelles by luminescence.
739 Cell Calcium. 2015;58:558-64.
740 65. Konieczny V, Keebler MV, Taylor CW. Spatial organization of intracellular Ca^{2+}
741 signals. Semin Cell Dev Biol. 2012;23:172-80.
742 66. Langeberg LK, Scott JD. Signalling scaffolds and local organization of cellular
743 behaviour. Nat Rev Mol Cell Biol. 2015;16:232-44.
744 67. Ariotti N, Rae J, Giles N, Martel N, Sierecki E, Gambin Y, et al. Ultrastructural
745 localisation of protein interactions using conditionally stable nanobodies. PLoS Biol.
746 2018;16:e2005473.
747 68. Rost BR, Schneider-Warme F, Schmitz D, Hegemann P. Optogenetic tools for
748 subcellular applications in neuroscience. Neuron. 2017;96:572-603.
749 69. Ruggiu AA, Bannwarth M, Johnsson K. Fura-2FF-based calcium indicator for protein
750 labeling. Org Biomol Chem. 2010;8:3398-401.
751 70. Kamiya M, Johnsson K. Localizable and highly sensitive calcium indicator based on a
752 BODIPY fluorophore. Anal Chem. 2010;82:6472-9.
753 71. Bannwarth M, Correa IR, Sztretye M, Pouvreau S, Fellay C, Aebischer A, et al. Indo-1
754 derivatives for local calcium sensing. ACS Chem Biol. 2009;4:179-90.
755 72. Wang C, Song X, Xiao Y. SNAP-tag-based subcellular protein labeling and fluorescent
756 imaging with naphthalimides. ChemBioChem. 2017;18:1762-9.

73. Abo M, Minakami R, Miyano K, Kamiya M, Nagano T, Urano Y, et al. Visualization of phagosomal hydrogen peroxide production by a novel fluorescent probe that is localized via SNAP-tag labeling. Anal Chem. 2014;86:5983-90.

74. Zimmermann M, Cal R, Janett E, Hoffmann V, Bochet CG, Constable E, et al. Cell-permeant and photocleavable chemical inducer of dimerization. Angew Chem Int Ed Engl. 2014;53:4717-20.

75. Feng S, Laketa V, Stein F, Rutkowska A, MacNamara A, Depner S, et al. A rapidly reversible chemical dimerizer system to study lipid signaling in living cells. Angew Chem Int Ed Engl. 2014;53:6720-3.

76. Putyrski M, Schultz C. Protein translocation as a tool: The current rapamycin story. FEBS Lett. 2012;586:2097-105.

77. Marschall AL, Dubel S, Boldicke T. Specific in vivo knockdown of protein function by intrabodies. MAbs. 2015;7:1010-35.

78. Michelangeli F, Ogunbayo OA, Wootton LL. A plethora of interacting organellar Ca^{2+} stores. Curr Opin Cell Biol. 2005;17:135-40.

79. Wong AK, Capitanio P, Lissandron V, Bortolozzi M, Pozzan T, Pizzo P. Heterogeneity of Ca^{2+} handling among and within Golgi compartments. J Mol Cell Biol. 2013;5:266-76.

80. Crevenna AH, Blank B, Maiser A, Emin D, Prescher J, Beck G, et al. Secretory cargo sorting by Ca^{2+}-dependent Cab45 oligomerization at the trans-Golgi network. J Cell Biol. 2016;213:305-14.

81. Appenzeller C, Andersson H, Kappeler F, Hauri HP. The lectin ERGIC-53 is a cargo transport receptor for glycoproteins. Nat Cell Biol. 1999;1:330-4.

780 82. Mitchell KJ, Pinton P, Varadi A, Tacchetti C, Ainscow EK, Pozzan T, et al. Dense core
781 secretory vesicles revealed as a dynamic Ca^{2+} store in neuroendocrine cells with a
782 vesicle-associated membrane protein aequorin indicator. J Cell Biol. 2001;155:41-51.
783 83. Mundorf ML, Troyer KP, Hochstetler SE, Near JA, Wightman RM. Vesicular Ca^{2+}
784 participates in the catalysis of exocytosis. J Biol Chem. 2000;275:9136-42.
785 84. Harmansa S, Affolter M. Protein binders and their applications in developmental
786 biology. Development. 2018;145:dev148874.
787 85. Tiede C, Bedford R, Heseltine SJ, Smith G, Wijetunga I, Ross R, et al. Affimer proteins
788 are versatile and renewable affinity reagents. eLife. 2017;6:e24903.
789 86. Sha F, Salzman G, Gupta A, Koide S. Monobodies and other synthetic binding proteins
790 for expanding protein science. Protein Sci. 2017;26:910-24.
791 87. Wozniak MJ, Bola B, Brownhill K, Yang YC, Levakova V, Allan VJ. Role of kinesin-1
792 and cytoplasmic dynein in endoplasmic reticulum movement in VERO cells. J Cell Sci.
793 2009;122:1979-89.
794 88. Lopez Sanjurjo CI, Tovey SC, Prole DL, Taylor CW. Lysosomes shape Ins(1,4,5)P_3-
795 evoked Ca^{2+} signals by selectively sequestering Ca^{2+} released from the endoplasmic
796 reticulum. J Cell Sci. 2013;126:289-300.
797 89. Brailoiu E, Churamani D, Cai X, Schrlau MG, Brailoiu GC, Gao X, et al. Essential
798 requirement for two-pore channel 1 in NAADP-mediated calcium signaling. J Cell
799 Biol. 2009;186:201-19.
800 90. Kanda T, Sullivan KF, Wahl GM. Histone-GFP fusion protein enables sensitive
801 analysis of chromosome dynamics in living mammalian cells. Curr Biol. 1998;8:377-
802 85.
803 91. English AR, Voeltz GK. Rab10 GTPase regulates ER dynamics and morphology. Nat
804 Cell Biol. 2013;15:169-78.

805 92. Cheeseman LP, Harry EF, McAinsh AD, Prior IA, Royle SJ. Specific removal of
806 TACC3-ch-TOG-clathrin at metaphase deregulates kinetochore fiber tension. J Cell
807 Sci. 2013;126:2102-13.
808 93. Goedhart J, von Stetten D, Noirclerc-Savoye M, Lelimousin M, Joosen L, Hink MA, et
809 al. Structure-guided evolution of cyan fluorescent proteins towards a quantum yield of
810 93%. Nat Commun. 2012;3:751.
811 94. Violin JD, Ren XR, Lefkowitz RJ. G-protein-coupled receptor kinase specificity for b-
812 arrestin recruitment to the b_2-adrenergic receptor revealed by fluorescence resonance
813 energy transfer. J Biol Chem. 2006;281:20577-88.
814 95. Schindelin J, Arganda-Carreras I, Frise E, Kaynig V, Longair M, Pietzsch T, et al. Fiji:
815 an open-source platform for biological-image analysis. Nat Methods. 2012;9:676-82.
816 96. Jaqaman K, Loerke D, Mettlen M, Kuwata H, Grinstein S, Schmid SL, et al. Robust
817 single-particle tracking in live-cell time-lapse sequences. Nat Methods. 2008;5:695-
818 702.
819 97. Bolte S, Cordelieres FP. A guided tour into subcellular colocalization analysis in light
820 microscopy. J Microsc. 2006;224:213-32.
821
822

Fig 1. Nanobody fusions for visualizing and manipulating intracellular signalling. Plasmids were generated that encode nanobodies specific for GFP variants (GNab) or RFP variants (RNab), fused to functional modules. Nanobody fusions with an N-terminal signal sequence to target them to the secretory pathway are also shown (ss-GNab and ss-RNab).

Fig 2. RNab and GNab fusion proteins bind to their respective tagged proteins in live cells. (**A**) Schematic of the RNab-GFP fusion binding to RFP. (**B**) HeLa cells expressing RNab-GFP with RFP-tagged markers for the ER surface (mCh-Sec61β), the mitochondrial surface (TOM20-mCh), the nucleus (H2B-mCh) or the surface of lysosomes (TPC2-mRFP). Cells were imaged in HBS using epifluorescence microscopy (cells expressing H2B-mCh) or TIRFM (other cells). Yellow boxes indicate regions enlarged in the subsequent panels. Colocalization values (Pearson's coefficient, *r*) were: mCh-Sec61β ($r = 0.93 \pm 0.09$, n = 10 cells); TOM20-mCh ($r = 0.94 \pm 0.09$, n = 10 cells); H2B-mCh ($r = 0.97 \pm 0.06$, n = 10 cells) and TPC2-mRFP ($r = 0.78 \pm 0.09$, n = 5 cells). (**C**) Schematic of the GNab-mCh fusion binding to GFP. (**D**) HeLa cells co-expressing GNab-mCh with GFP-tagged markers for the ER surface (GFP-ERcyt), the mitochondrial surface (TOM20-GFP) and the nucleus (H2B-GFP), or an mTurquoise2-tagged ER-surface marker (mTurq-ERcyt). Cells were imaged using epifluorescence microscopy (cells expressing H2B-GFP) or TIRFM (other cells). Yellow boxes indicate regions enlarged in the subsequent panels. Colocalization values were: GFP-ERcyt ($r = 0.92 \pm 0.08$, n = 8 cells); TOM20-GFP ($r = 0.87 \pm 0.05$, n = 7 cells); H2B-GFP ($r = 0.94 \pm 0.07$, n = 6 cells) and mTurq-ERcyt ($r = 0.97 \pm 0.03$, n = 7 cells). Scale bars 10 µm (main images) or 2.5 µm (enlargements).

Fig 3. Targeting RNab-Ca^{2+} sensors to RFP-tagged proteins. (**A**) Schematic of RNab-GGECO fusion binding to RFP. (**B-D**) HeLa cells expressing RNab-GGECO1.2 and TOM20-mCh, before and after addition of histamine (100 μM) and then ionomycin (5 μM). Cells were imaged in HBS using TIRFM. The TOM20-mCh image is shown after the histamine and ionomycin additions. The merged images are shown using images of RNab-GGECO1.2 after ionomycin (B, C) or histamine (D). The yellow and cyan boxed regions in panel B are shown enlarged in panels C and D, respectively. Scale bars are 10 μm (B) or 1.25 μm (C, D). (**E**) Timecourse of the effects of histamine (100 μM) and ionomycin (5 μM) on the fluorescence of RNab-GGECO1.2 (F/F_0, where F and F_0 are fluorescence recorded at t and t = 0). The traces are from regions coinciding with a single mitochondrion or cytosol (regions identified in panel D), indicating changes in [Ca^{2+}] at the OMM. (**F**) Enlarged region (70-180 s) of the graph shown in E. Results are representative of cells from 13 independent experiments.

Fig 4. Targeted GNab-Ca^{2+} sensors detect changes in [Ca^{2+}] at the surface of mitochondria. (**A**) Schematic of GNab-RGECO fusions binding to GFP. (**B, C**) Representative HeLa cells co-expressing TOM20-GFP and GNab-RGECO1.2 imaged in HBS using TIRFM before and after addition of histamine (100 μM) and then ionomycin (5 μM). The TOM20-GFP images are shown after the histamine and ionomycin additions. Histamine and ionomycin evoked changes in fluorescence of GNab-RGECO1.2 at the OMM. (**D-F**) Similar analyses of HeLa cells co-expressing TOM20-GFP and and GNab-LAR-GECO1.2 (GNab-LARG1.2). Histamine (100 μM) evoked changes in fluorescence of GNab-LARG1.2 at the OMM of mitochondria in the perinuclear region (region of interest 1 (ROI 1) in E), but not in a peripheral region (ROI 2 in F). All mitochondria responded to ionomycin (5 μM), indicating that histamine evoked local changes in [Ca^{2+}] at the OMM. The cyan and yellow boxed regions in D are shown enlarged in E and F, respectively. Scale bars 10 μm (B, D) or 2.5 μm (C, E, F). (**G**) Timecourse of the changes in fluorescence of GNab-RGECO1.2 at the OMM evoked by histamine and ionomycin for the entire cell shown in B. (**H**) Fluorescence changes recorded from ROI 1 and ROI 2 in panels E and F. Results are representative of cells from 4 independent experiments.

Fig 5. Targeting H^+ sensors to RFP-tagged and GFP-tagged proteins. (**A**) Schematic of RNab fused to the pH sensor superecliptic pHluorin (RNab-SEpH) and bound to RFP. (**B**) Schematic of GNab-pHuji binding to RFP. (**C**, **D**) HeLa cells co-expressing RNab-SEpH and TOM20-mCh were imaged in modified HBS (MHBS) using epifluorescence microscopy and exposed to extracellular pH 6.5 (C) or pH 8 (D) in the presence of nigericin (10 μM). Scale bars 10 μm. (**E, F**) HeLa cells co-expressing GNab-pHuji and TOM20-GFP were exposed to extracellular pH 6.5 (E) or pH 8 (F) in the presence of nigericin. Scale bars 10 μm. (**G**, **H**) Timecourse from single cells of the fluorescence changes (F/F_0) of mitochondrially targeted RNab-SEpH or GNab-pHuji evoked by the indicated manipulations of extracellular pH. Results shown are representative of 3 independent experiments.

Fig 6. Targeting an ATP/ADP sensor to RFP-tagged proteins. (**A**) Schematic of RNab-Perceval-HR fusion (RNab-PHR) bound to RFP. (**B**) HeLa cells co-expressing RNab-PHR and TOM20-mCh were imaged in HBS using epifluorescence microscopy. The yellow box indicates the region enlarged in subsequent panels. Scale bars 10 μm (main image) and 2.5 μm (enlarged images). (**C, D**) Changes in fluorescence for each excitation wavelength (405 and 488 nm, F/F_0) (C) and their ratio (R/R_0, where $R = F_{405}/F_{488}$) (D) of mitochondrially targeted RNab-PercevalHR after addition of 2-deoxyglucose (2DG, 10 mM), oligomycin (OM, 1 μM) and antimycin (AM, 1 μM). The results indicate a decrease in the ATP/ADP ratio at the OMM. Results are representative of 3 independent experiments.

Fig 7. Nanobody-SNAPf fusion proteins allow labelling of RFP-tagged and GFP-tagged proteins with fluorescent O^6-benzylguanine derivatives in live cells. (**A, B**) Schematics of RNab-SNAPf fusion bound to RFP, and GNab-SNAPf fusion bound to GFP, after labelling with SNAP-Cell-647-SiR (magenta circles). (**C-F**) HeLa cells co-expressing RNab-SNAPf and mitochondrial TOM20-mCh (C), RNab-SNAPf and lysosomal LAMP1-mCh (D), GNab-SNAPf and TOM20-GFP (E) or GNab-SNAPf and LAMP1-GFP (F) were treated with SNAP-Cell-647-SiR (0.5 µM, 30 min at 37ºC) and imaged using TIRFM. Scale bars 10 µm (main images) or 2.5 µm (enlarged images). Colocalization values: RNab-SNAPf + TOM20-mCh (r = 0.95 ± 0.02, n = 6 cells); RNab-SNAPf + LAMP1-mCh (r = 0.84 ± 0.06, n = 8 cells); GNab-SNAPf + TOM20-GFP (r = 0.78 ± 0.09, n = 10 cells); and GNab-SNAPf + LAMP1-GFP (r = 0.85 ± 0.10, n = 11 cells).

Fig 8. Targeting CALI to lysosomes using RNab-SNAPf reduces lysosomal motility. (**A**) Schematic of RNab-SNAPf after labelling with SNAP-Cell-fluorescein (green circle) and bound to RFP. (**B**) HeLa cells co-expressing LAMP1-mCh and RNab-SNAPf were incubated with SNAP-Cell-fluorescein (0.5 µM, 30 min, 37ºC), which labelled lysosomes (colocalization values, $r = 0.73 \pm 0.02$, n = 6 cells), and imaged using TIRFM. (**C, D**) Cells were then exposed to 488-nm light for 3 s to induce CALI. TIRFM images show a representative cell at different times before (C) and after (D) CALI, with the image at t = 0 s shown in magenta and the image at t = 60 s in green. White in the merged image indicates immobile lysosomes, while green and magenta indicate lysosomes that moved in the interval between images. Yellow boxes show regions enlarged in subsequent images. Scale bars 10 µm (main images) and 2.5 µm (enlargements). For clarity, images were auto-adjusted for brightness and contrast (ImageJ) to compensate for bleaching of mCh during tracking and CALI. (**E**) Effect of CALI on the displacements of individual lysosomes, determining by particle-tracking (TrackMate), during a 60-s recording from a representative cell (images taken every 1 s). (**F**) Summary data (mean ± SEM, n = 6 cells from 6 independent experiments) show the mean fractional decrease in displacement (ΔDisplacement) due to CALI in cells expressing RNab-SNAPf or cytosolic SNAPf (see ***Additional file 1: Fig. S2***). The fractional decrease in displacement for each cell was defined as: $(MD_{pre} - MD_{post}) / MD_{pre}$, where MD_{pre} and MD_{post} are the mean displacement of all tracked particles in 60 s before and after CALI. $^{*}p < 0.05$, unpaired Student's *t*-test.

925 **Fig 9. Clustering of RFP-tagged and GFP-tagged proteins and organelles using RNab-**
926 **mCerulean-MP and GNab-mRFP-MP.** (**A**) Schematic of RNab-mCerulean-MP fusion
927 bound to RFP. (**B**) Schematic of GNab-mRFP-MP fusion bound to GFP. (**C-F**) HeLa cells
928 expressing RFP-tagged proteins in the absence (**C, E**) or presence (**D**, **F**) of co-expressed
929 RNab-mCerulean-MP (RNab-mCer-MP) were imaged using epifluorescence microscopy. (**G-**
930 **N**) HeLa cells expressing GFP-tagged proteins in the absence (G, I, K, M) or presence (H, J,
931 L, N) of co-expressed GNab-mRFP-MP were imaged using epifluorescence microscopy.
932 Results are representative of at least 5 cells, from at least 3 independent experiments. Scale
933 bars 10 µm.

Fig 10. RNab-FKBP inducibly recruits ER transmembrane proteins to mitochondria. (**A**) Schematic of RNab-FKBP bound to RFP. (**B**) Schematic of GNab-FKBP bound to GFP. (**C, D**) HeLa cells co-expressing RNab-FKBP, mitochondrial TOM70-GFP-FRB and mCh-Sec61β were imaged using TIRFM. A representative cell (n = 7) is shown before (C) and after (D) treatment with rapamycin (100 nM, 10 min). The boxed region is enlarged in subsequent images. Scale bars 10 μm (main images) and 2.5 μm (enlargements). (**E**) Timecourse of mCh-Sec61β fluorescence changes (F/F_0) evoked by rapamycin recorded at a representative mitochondrion and in nearby reticular ER. Results show ~80% loss of fluorescence from the ER devoid of mitochondrial contacts. (**F**, **G**) HeLa cells co-expressing endogenously tagged GFP-IP_3R1, GNab-FKBP and mitochondrial TOM70-mCh-FRB were imaged using TIRFM. A representative cell (n = 6) is shown before (F) and after (G) treatment with rapamycin (100 nM, 10 min). The boxed region is enlarged in subsequent images. Scale bars 10 μm (main images) and 2.5 μm (enlargements). (**H**) HeLa cells co-expressing GFP-calmodulin (GFP-CaM), GNab-FKBP and TOM20-mCh-FRB were imaged using epifluorescence microscopy. A representative cell (n = 3) is shown before and after treatment with rapamycin (100 nM, 10 min). The image for TOM-mCh-FRB is shown in the presence of rapamycin. Scale bar 10 μm.

Fig 11. Reversible optogenetic recruitment of RFP-tagged proteins using RNab-zdk1. (**A**) Schematic of RNab-zdk1 fusion bound to RFP, showing the reversible light-evoked dissociation of zdk1 from LOV2. (**B**) HeLa cells co-expressing RNab-zdk1, mitochondrial TOM20-LOV2 and cytosolic mCh were imaged using TIRFM. A representative cell is shown before and after one or five 1-s exposures to blue light (488-nm laser at 2-s intervals) and after a 3-min recovery period in the dark. Scale bar 10 μm. (**C**) Timecourse of the mCherry fluorescence changes (F/F_0) recorded at a representative mitochondrion and in nearby cytosol after each of the indicated light flashes. There is a reversible decrease (~60%) in mitochondrial mCh fluorescence and a corresponding reversible increase (~70%) in cytosolic fluorescence. A single measurement of mCh fluorescence was made at the end of a 3-min recovery period in the dark (REC) before further light flashes. Results are representative of 5 cells from 3 independent experiments.

Fig 12. Recruitment of proteins to native PM-mitochondria MCS using RNab-FKBP. (**A**) Schematic of RNab-FKBP fusion bound to RFP. (**B, C**) HeLa cells co-expressing RNab-FKBP, mitochondrial TOM70-GFP-FRB and β_2AR-mCh were imaged using TIRFM before (B) and after (C) treatment with rapamycin (100 nM, 10 min). Scale bar 10 μm. (**D, E**) Enlarged images from C of the yellow box (D) and cyan box (E) show punctate recruitment of β_2AR-mCh to individual mitochondria at the indicated times after addition of rapamycin. Scale bars 1.25 μm. (**F**) TIRFM images of HeLa cells co-expressing mitochondrial TOM70-GFP-FRB and β_2AR-mCh in the presence of rapamycin (100 nM, 10 min) show no recruitment in the absence of co-expressed RNab-FKBP. The yellow box shows a region enlarged in the subsequent image. Scale bars 10 μm (main images) and 2.5 μm (enlargement). Results (B-F) are representative of 5 independent experiments.

Fig 13. Recruitment of PM proteins to ER-PM MCS using RNab-FKBP. (**A**) Schematic of RNab-FKBP fusion bound to RFP. (**B**) HeLa cells co-expressing RNab-FKBP, mCh-Orai1 and the ER-PM junction marker GFP-MAPPER-FRB were imaged using TIRFM. A representative cell (n = 5) is shown before (top row) and after (bottom row) treatment with rapamycin (100 nM, 10 min). The boxed region is shown enlarged in subsequent images. (**C**) HeLa cells co-expressing mCh-Orai1 and GFP-MAPPER-FRB alone were imaged using TIRFM. A representative cell (n = 3) is shown before (top row) and after (bottom row) treatment with rapamycin (100 nM, 10 min). The boxed region is shown enlarged in subsequent images. The results show no recruitment in the absence of co-expressed RNab-FKBP. Scale bars (B, C) 10 μm (main images) and 2.5 μm (enlargements).

Fig 14. Inducible recruitment of lysosomes to mitochondria using GNab-FKBP. (**A**) Schematic of GNab-FKBP fusion bound to GFP. (**B**) HeLa cells co-expressing mitochondrial TOM70-mCh-FRB (magenta), lysosomal LAMP1-GFP (green) and GNab-FKBP were imaged using TIRFM. Merged images of a representative cell (n = 5) are shown before and at times after treatment with rapamycin (rapa, 100 nM). Scale bar 10 μm. (**C**) Enlargements of the boxed region in (B). Scale bar 2.5 μm. (**D**) HeLa cells co-expressing TOM70-mCh-FRB (magenta) and lysosomal LAMP1-GFP (green) were imaged using TIRFM. A representative cell (n = 3) is shown before and after treatment with rapamycin (100 μm, 10 min); there is no recruitment in the absence of co-expressed GNab-FKBP. The yellow box shows a region enlarged in the subsequent image. Scale bars 10 μm (main images) and 2.5 μm (enlargement).

Fig 15. Crosslinking GFP-tagged and RFP-tagged proteins and organelles using GNab-RNab. (**A**) Schematic of GNab-RNab bound to GFP and RFP. (**B-E**) HeLa cells co-expressing the tagged proteins indicated with GNab-RNab were imaged using epifluorescence microscopy (B) or TIRFM (C-E). Representative cells (n = 5-7) are shown. Control images for GFP-IP_3R1 are shown in ***Fig. 10*** and ***Additional file 1: Fig S3***. (**F, G**) HeLa cells co-expressing LAMP1-GFP and LAMP1-mCh in the absence (F) or presence (G) of co-expressed GNab-RNab were imaged using TIRFM. Representative cells (n = 5) are shown. Scale bars (B-G) 10 µm (main images) and 2.5 µm (enlargements of boxed areas).

Fig 16. Inducible crosslinking of RFP-tagged and GFP-tagged proteins with GNab-FKBP and RNab-FRB. (**A**) Schematic of the nanobody fusions used, with rapamycin shown as a blue sphere. (**B**, **C**) HeLa cells co-expressing GNab-FKBP, RNab-FRB, TOM20-GFP and mCh-Sec61β were imaged using TIRFM. A representative cell (n = 3) is shown before (B) and after (C) treatment with rapamycin (100 nM, 10 min). Scale bars 10 µm (main images) and 2.5 µm (enlargements of boxed areas).

Fig 17. Nanobody fusions can be targeted to different lumenal compartments of the secretory pathway. (**A**) Schematic of ssGNab-mCh bound to GFP. (**B**) HeLa cells co-expressing ssGNab-mCh and either the lumenal ER marker mTurquoise2-ERlumen, the marker of ER-PM junctions GFP-MAPPER, or the Golgi marker GFP-Golgi. Cells were imaged using epifluorescence microscopy. Representative cells are shown. Colocalization values were: mTurquoise2-ERlumen (r = 0.96 ± 0.03, n = 10); GFP-MAPPER (r = 0.94 ± 0.02, n = 5); and GFP-Golgi (r = 0.91 ± 0.06, n = 4). (**C**) Schematic of ssRNab-GFP bound to RFP. (**D**) HeLa cells co-expressing ssRNab-GFP and either mCh-ERlumen or mCh-MAPPER were imaged using epifluorescence microscopy. Representative cells are shown. Colocalization values were: mCh-ERlumen (r = 0.98 ± 0.009, n = 9) and mCh-MAPPER (r = 0.93 ± 0.07, n = 13. Scale bars 10 μm (main images) and 2.5 μm (enlargements).

Fig 18. Nanobody-mediated targeting of low-affinity Ca^{2+} sensors allows measurement of changes in [Ca^{2+}] in an ER sub-compartment at ER-PM MCS. (**A**) Schematic of ssRNab-Ca^{2+} sensor bound to RFP. (**B**) Schematic of ssGNab-Ca^{2+} sensor bound to GFP. (**C-F**) HeLa cells co-expressing the indicated combinations of mCh-MAPPER, GFP-MAPPER, ssRNab-GCEPIA (ssRNab-GC), ssRNab-GEMCEPIA (ssRNab-GEM; image is shown for the 525-nm emission channel), ssGNab-LAR-GECO1 (ssGNab-LGECO) or ssGNab-RCEPIA were imaged in Ca^{2+}-free HBS using TIRFM. Yellow boxes indicate regions enlarged in subsequent images. Scale bars 10 µm (main images) and 2.5 µm (enlargements). (**G-J**) Timecourses of fluorescence changes recorded from cells co-expressing mCh-MAPPER and ssRNab-GCEPIA (G), mCh-MAPPER and ssRNab-GEMCEPIA (H), GFP-MAPPER and ssGNab-LAR-GECO1 (ssGNab-LARG1) (I) and GFP-MAPPER and ssGNab-RCEPIA (J) in response to emptying of intracellular Ca^{2+} stores with ionomycin (5 µM). (**K**) Summary results (mean ± SD, n = 4 cells) show mean fractional decreases (ΔF) in either fluorescence or emission ratio (for ssRNab-GEM) recorded 90 s after addition of ionomycin.

Additional files

Additional file 1 (.pptx): Figures S1-S6

Fig. S1 Targeting RNab-GEMGECO Ca^{2+} sensor to RFP-tagged proteins. (**A**) Schematic of RNab-GEMGECO fusion binding to RFP. (**B**) HeLa cells co-expressing RNab-GEMGECO and TOM20-mCh were imaged in HBS using TIRFM. Images are shown before and after addition of histamine (100 µM) and then ionomycin (5 µM). The TOM20-mCh and merged images are before additions of histamine and ionomycin. The yellow boxed region in shown enlarged in (C). Scale bar 10 µm. (**C**) Enlarged regions from (B). Scale bar 2.5 µm. (**D**, **E**) Representative timecourses of histamine and ionomycin-evoked changes in fluorescence (D) and fluorescence emission ratio ($R/R_0 = F_{480}/F_{525}$) (E) of mitochondrially targeted RNab-GEMGECO. Results are representative of cells from 4 independent experiments.

Fig. S2 Targeting CALI to lysosomes with SNAP-Cell-fluorescein: cytosolic controls. (**A**) Schematic of cytosolic SNAPf, which does not bind to RFP, after its labelling with SNAP-Cell-fluorescein. (**B-D**) HeLa cells co-expressing LAMP1-mCh and cytosolic SNAPf (Cyt-SNAPf) were treated with SNAP-Cell-fluorescein (0.5 µM, 30 min, 37ºC) and imaged using TIRFM. Scale bar 10 µm. Cells were then exposed to 488-nm light for 3 s to induce CALI. Images show a representative cell at different times before (C) and after (D) CALI, with the image at t = 0 s shown in magenta and the image at t = 60 s in green. White in the merged image indicates immobile lysosomes, while green and magenta indicate lysosomes that moved during the 60 s between images. Yellow boxes show regions enlarged in subsequent images. Scale bars 10 µm (main images) and 2.5 µm (enlargements). For clarity, images were auto-adjusted for brightness and contrast (ImageJ) to compensate for bleaching of mCh during tracking and CALI. (**E**) Displacements of individual lysosomes during a 60-s recording (determined by TIRFM using TrackMate, with images taken every 1 s) for a representative HeLa cell co-expressing LAMP1-mCh and cytosolic SNAPf before and after CALI (3-s exposure to 488-nm light). Typical of n = 6 cells. Summary data are shown in ***Fig. 8F***.

Fig. S3 Rapamycin alone does not recruit RFP-tagged or GFP-tagged proteins to mitochondria. (**A, B**) HeLa cells co-expressing mitochondrial TOM70-mCh-FRB and mCh-Sec61β were imaged using TIRFM before (A) and after (B) addition of rapamycin (100 nM, 10 min). (**C, D**) HeLa cells co-expressing endogenously tagged GFP-IP_3R1 and mitochondrial TOM70-mCh-FRB were imaged using TIRFM before (C) and after (D) addition of rapamycin (100 nM, 10 min). (**E**) HeLa cells co-expressing GFP-calmodulin (GFP-CaM) and mitochondrial TOM70-mCh-FRB were imaged using TIRFM before and after addition of rapamycin (100 nM, 10 min). Results are each representative of cells from 3-5 independent experiments. Scale bars 10 µm (main images) and 2.5 µm (enlargements).

Fig. S4 Recruitment of proteins to native PM-mitochondria MCS using GNab-FKBP. (**A**) Schematic of GNab-FKBP fusion bound to GFP. (**B**) TIRFM images of COS-7 cells co-expressing GNab-FKBP, β_2AR-GFP and TOM70-mCh-FRB. A representative cell (n = 3) is shown before (top row) and at the indicated times after addition of rapamycin (100 nM). Scale bar 10 µm. (**C**) Enlargements of the boxed regions in (B). Scale bar 3.75 µm.

Fig. S5 Inducible crosslinking of RFP-tagged and GFP-tagged proteins with RNab-FKBP and GNab-FRB. (**A**) Schematic of the nanobody fusions used, with rapamycin shown as a blue sphere. (**B, C**) HeLa cells co-expressing RNab-FKBP, GNab-FRB, TOM20-GFP and mCh-Sec61β were imaged using TIRFM. A representative cell (n = 3) is shown before (B) and after (C) treatment with rapamycin (100 nM, 10 min). Scale bars 10 µm (main images) and 2.5 µm (enlargements).

Fig. S6. DNA sequences encoding the nanobodies used.

Additional file 2 (.wmv): Video 1. RNab-GGECO1.2 detects changes in [Ca^{2+}] at the surface of mitochondria expressing TOM20-mCh. The top panel shows RNab-GGECO1.2 fluorescence (488-nm TIRFM excitation) and the bottom panel shows TOM20-mCh fluorescence (561-nm TIRFM excitation). In response to histamine (100 µM, added at 60 s), local rises in $[Ca^{2+}]_c$ were detected at the surfaces of individual mitochondria, but not in the bulk cytosol. Ionomycin (5 µM) was added at 3 min. Video was acquired at 1 Hz and is shown at 30 frames per second (fps). Clock is in min:s. Relates to ***Fig. 3D***.

Additional file 3 (.wmv): Video 2. GNab-LARGECO1.2 detects local changes in [Ca^{2+}] at the surface of mitochondria expressing TOM20-GFP. The video shows GNab-LARGECO1.2 fluorescence (488-nm TIRFM excitation). Histamine (100 µM, added at 60 s) causes local rises in $[Ca^{2+}]_c$ at the OMM of individual mitochondria in the perinuclear region (cyan box in ***Fig. 4D***), but not in peripheral regions (e.g. yellow box in ***Fig. 4D***). Ionomycin (5 µM) was added at 3 min. Video was acquired at 1 Hz and is shown at 33 fps. Clock is in min:s. Relates to ***Fig. 4D-F***.

Additional file 4 (.wmv): Video 3. Effect of targeted CALI on lysosomal motility. HeLa cells expressing LAMP1-mCh and RNab-SNAPf were imaged using TIRFM and 561-nm laser illumination before (top) and after (bottom) CALI (3.02 s exposure to 488-nm epifluorescence laser illumination). Video was acquired at 0.5 Hz and is shown at 3 fps. Clock is in min:s. Relates to ***Fig. 8***.

Additional file 5 (.wmv): Video 4. RNab-FKBP rapidly sequesters an ER integral membrane protein at the OMM. TIRFM images of HeLa cells expressing TOM70-GFP-FRB, RNab-FKBP and mCh-Sec61β were treated with rapamycin (100 nM, added at 60 s). The ER membrane protein, mCh-Sec61β , is then rapidly sequestered at the OMM. Video was acquired at 0.5 Hz and shown at 33 fps. Clock is in min:s. Relates to ***Fig. 10C*** and ***D***.

Additional file 6 (.wmv): Video 5. GNab-FKBP rapidly sequesters endogenously tagged GFP-IP$_3$R1 at the OMM. TIRFM images show HeLa cells with endogenously GFP-tagged IP$_3$R1 and transiently expressing TOM70-mCh-FRB and GNab-FKBP and then treated with rapamycin (100 nM, added at 60 s). GFP-IP$_3$R1 is rapidly sequestered at the OMM. Video was acquired at 0.5 Hz and is shown at 33 fps. Clock is in min:s. Relates to ***Fig. 10F*** and ***G***.

.

Additional file 7 (.wmv): Video 6. GNab-FKBP rapidly sequesters GFP-CaM at the OMM. Epifluorescence microscopy images show HeLa cells transiently expressing GFP-CaM, GNab-FKBP and TOM20-mCh-FRB, and then treated with rapamycin (100 nM, added at 60 s). GFP-CaM is rapidly sequestered at the OMM. Video was acquired at 0.5 Hz and is shown at 9 fps. Clock is in min:s. Relates to ***Fig. 10H***.

Additional file 8 (.wmv): Video 7. RNab-FKBP recruits a PM protein to the OMM in response to rapamycin. TIRFM images of HeLa cells expressing TOM70-GFP-FRB, RNab-FKBP and the PM protein, β_2AR-mCh, and then exposed to rapamycin (100 nM, added at 60 s). There is a rapid translocation of β_2AR-mCh to the OMM. Video was acquired at 0.5 Hz and is shown at 33 fps. Clock is in min:s. Relates to ***Fig. 12B-E***.

Additional file 9 (.wmv): Video 8. Crosslinking GNab-FKBP and RNab-FRB with rapamycin recruits mCh-Sec61β to TOM20-GFP in the OMM. HeLa cells expressing GNab-FKBP, RNab-FRB, mCh-Sec61β and TOM20-GFP were stimulated with rapamycin (100 nM, added at 100 s). The TIRFM images show rapid recruitment of mCh-Sec61β to the OMM. Video was acquired at 0.2 Hz and is shown at 8 fps. Clock is in min:s. Relates to ***Fig. 16***.

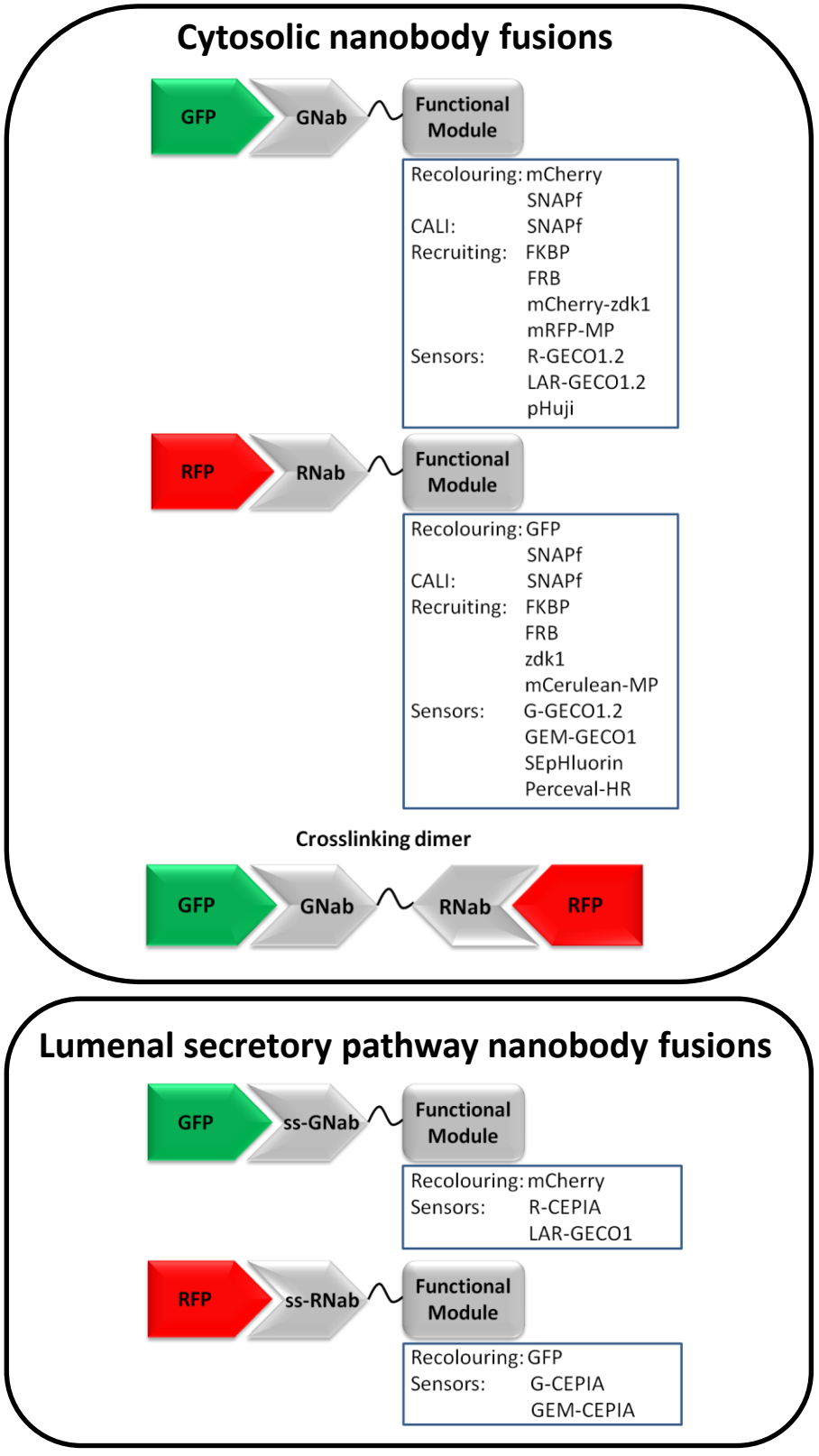
Cytosolic nanobody fusions
GFP
GNab
Functional Module
Recolouring: mCherry
SNAPf
CALI: SNAPf
Recruiting: FKBP
FRB
mCherry-zdk1
mRFP-MP
Sensors: R-GECO1.2
LAR-GECO1.2
pHuji
RFP
RNab
Functional Module
Recolouring: GFP
SNAPf
CALI: SNAPf
Recruiting: FKBP
FRB
zdk1
mCerulean-MP
Sensors: G-GECO1.2
GEM-GECO1
SEpHluorin
Perceval-HR
Crosslinking dimer
GFP
GNab
RNab
RFP
Lumenal secretory pathway nanobody fusions
GFP
ss-GNab
Functional Module
Recolouring: mCherry
Sensors: R-CEPIA
LAR-GECO1
RFP
ss-RNab
Functional Module
Recolouring: GFP
Sensors: G-CEPIA
GEM-CEPIA

Figure 1.

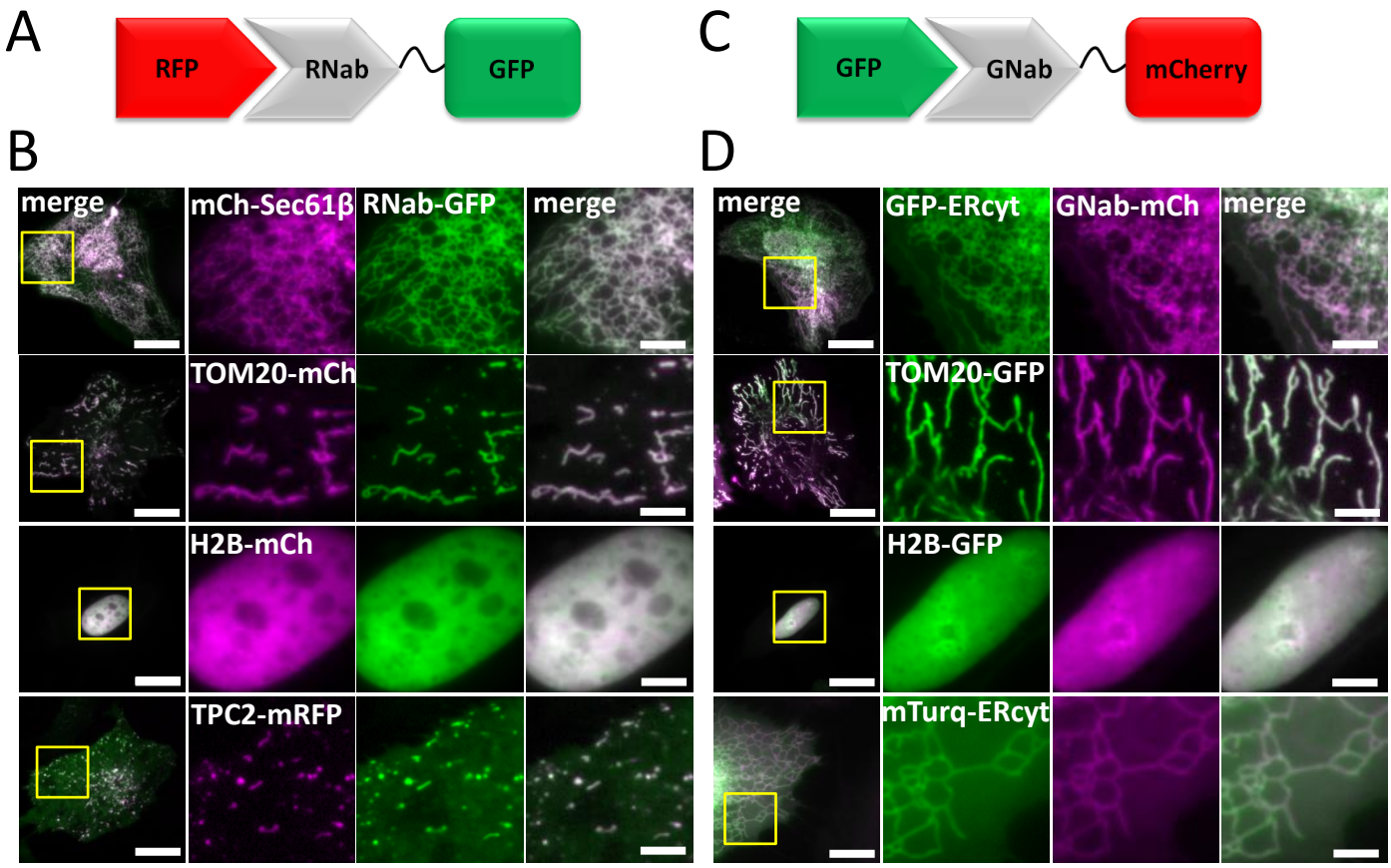
A
RFP
RNab
GFP
C
GFP
GNab
mCherry
B
merge
mCh-Sec61β
RNab-GFP
merge
TOM20-mCh
H2B-mCh
TPC2-mRFP
D
merge
GFP-ERcyt
GNab-mCh
merge
TOM20-GFP
H2B-GFP
mTurq-ERcyt

Figure 2.

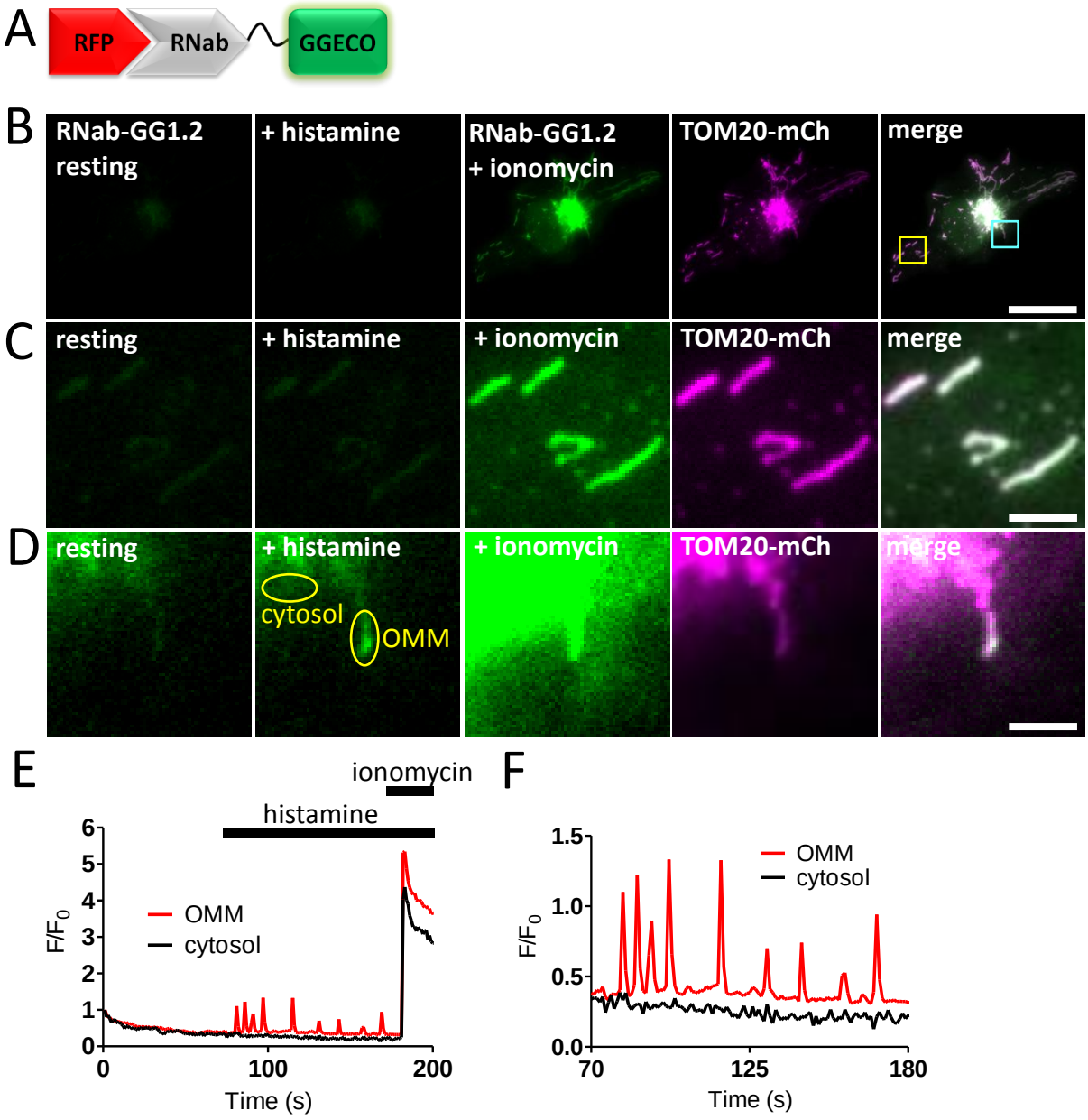
A
RFP
RNab
GGECO
B
RNab-GG1.2
resting
+ histamine
RNab-GG1.2
+ ionomycin
TOM20-mCh
merge
C
resting
+ histamine
+ ionomycin
TOM20-mCh
merge
D
resting
+ histamine
cytosol
OMM
+ ionomycin
TOM20-mCh
merge
E
ionomycin
histamine
OMM
cytosol
F/F0
Time (s)
F
OMM
cytosol
F/F0
Time (s)

Figure 3.

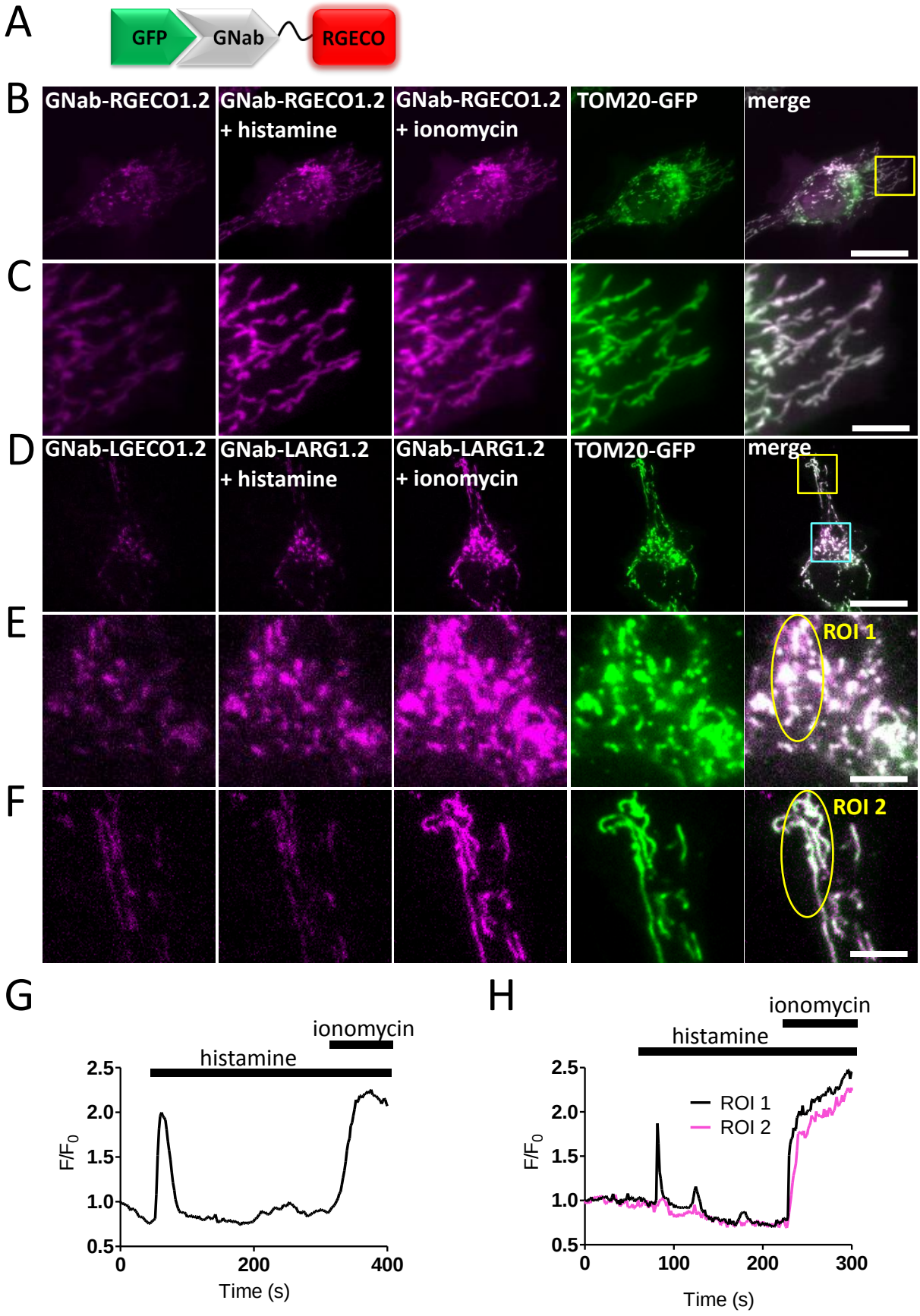
A
GFP
GNab
RGECO
B
GNab-RGECO1.2
GNab-RGECO1.2 + histamine
GNab-RGECO1.2 + ionomycin
TOM20-GFP
merge
C
D
GNab-LGECO1.2
GNab-LARG1.2 + histamine
GNab-LARG1.2 + ionomycin
TOM20-GFP
merge
E
ROI 1
F
ROI 2
G
ionomycin
histamine
F/F0
Time (s)
H
ionomycin
histamine
ROI 1
ROI 2
F/F0
Time (s)

Figure 4.

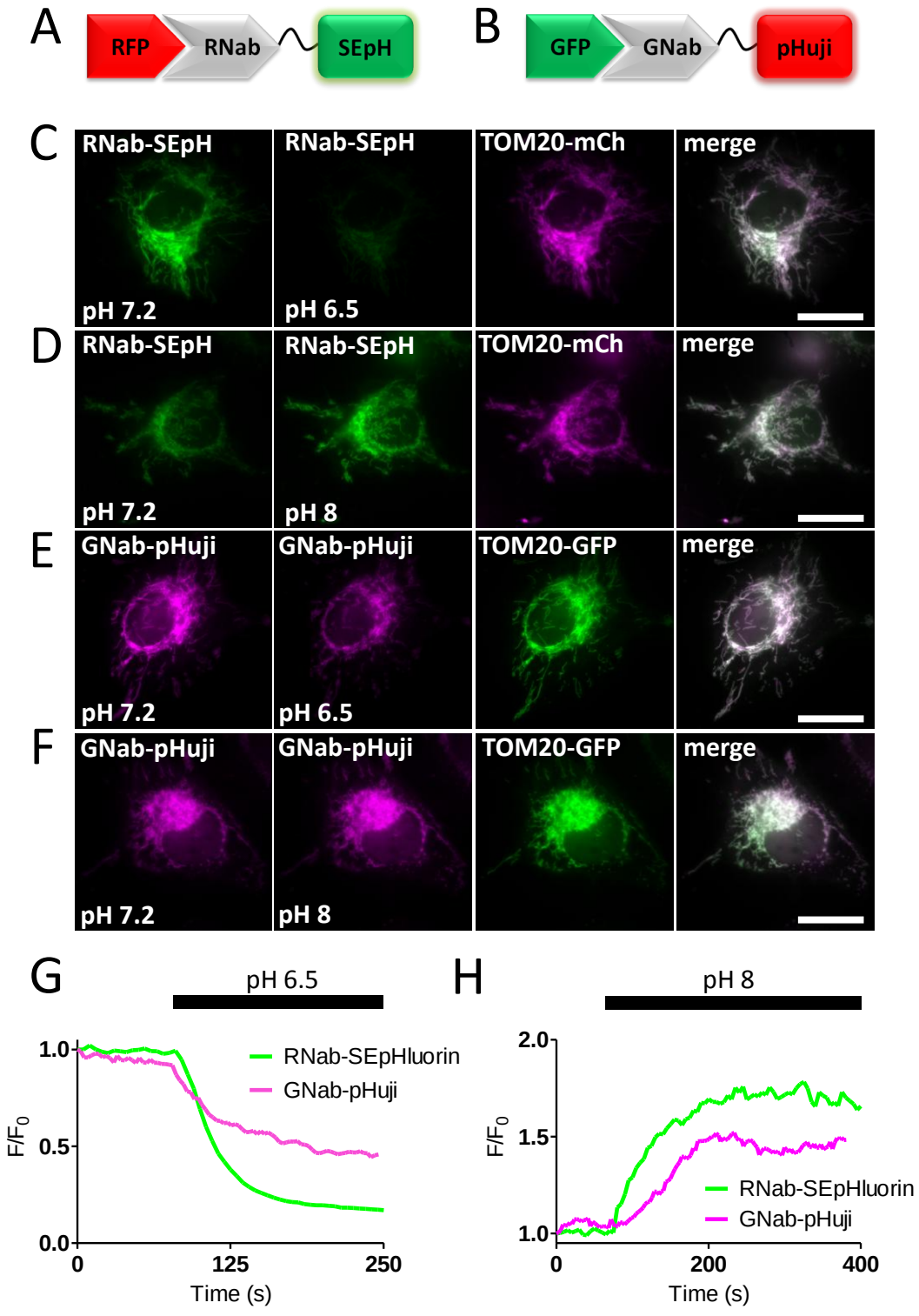
A
RFP
RNab
SEpH
B
GFP
GNab
pHuji
C
RNab-SEpH
pH 7.2
RNab-SEpH
pH 6.5
TOM20-mCh
merge
D
RNab-SEpH
pH 7.2
RNab-SEpH
pH 8
TOM20-mCh
merge
E
GNab-pHuji
pH 7.2
GNab-pHuji
pH 6.5
TOM20-GFP
merge
F
GNab-pHuji
pH 7.2
GNab-pHuji
pH 8
TOM20-GFP
merge
G
pH 6.5
RNab-SEpHluorin
GNab-pHuji
F/F0
1.0
0.5
0.0
0
125
250
Time (s)
H
pH 8
RNab-SEpHluorin
GNab-pHuji
F/F0
2.0
1.5
1.0
0
200
400
Time (s)

Figure 5.

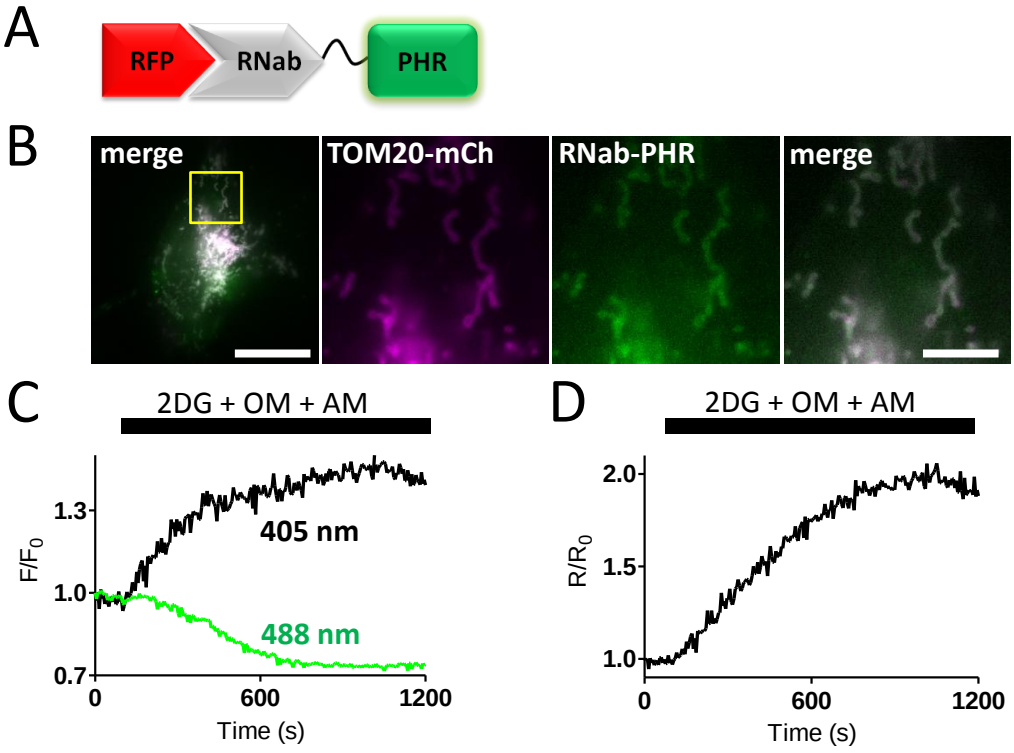
A
RFP
RNab
PHR
B
merge
TOM20-mCh
RNab-PHR
merge
C
2DG + OM + AM
405 nm
488 nm
F/F0
1.3
1.0
0.7
0
600
1200
Time (s)
D
2DG + OM + AM
R/R0
2.0
1.5
1.0
0
600
1200
Time (s)

Figure 6.

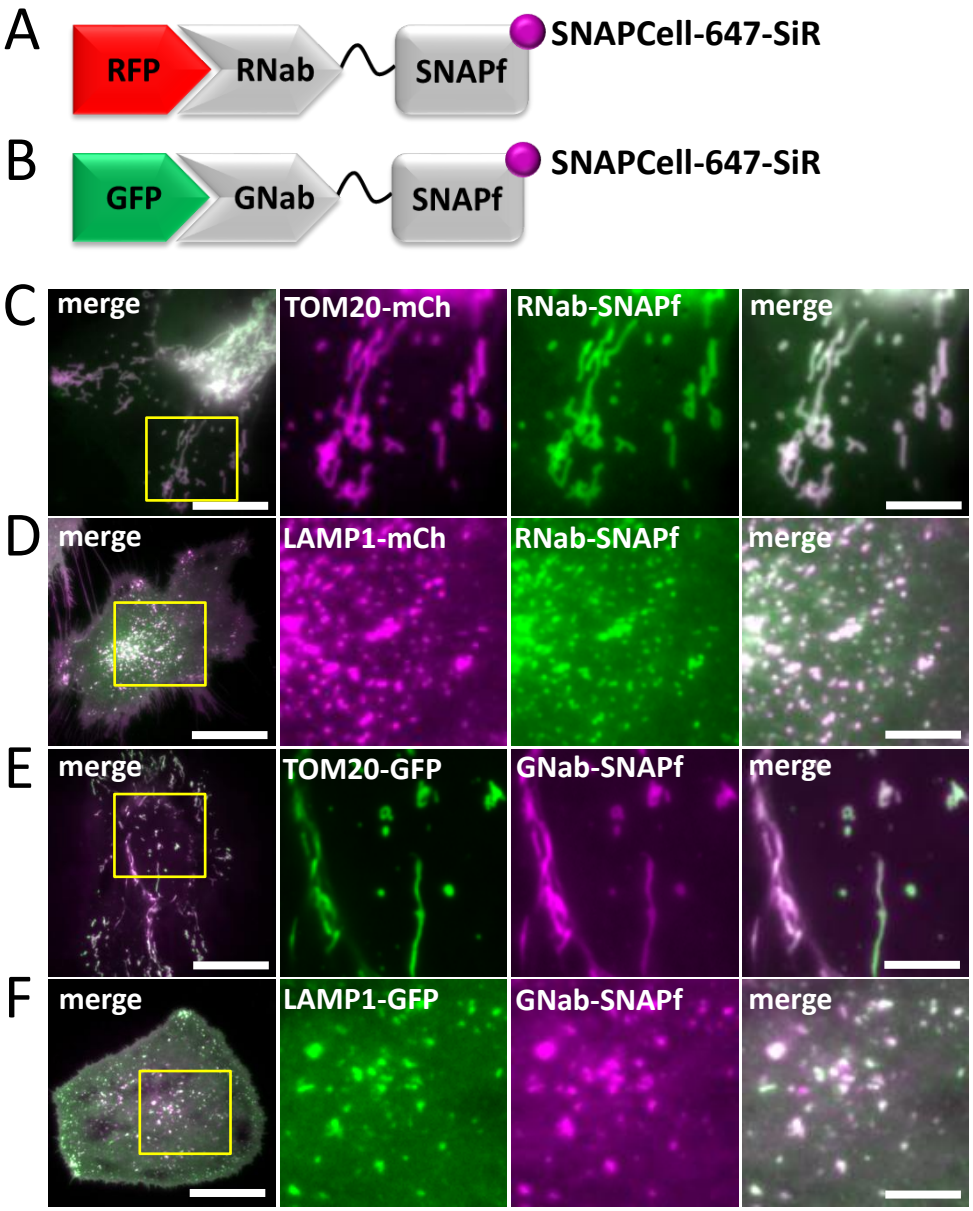
A
RFP
RNab
SNAPf
SNAPCell-647-SiR
B
GFP
GNab
SNAPf
SNAPCell-647-SiR
C
merge
TOM20-mCh
RNab-SNAPf
merge
D
merge
LAMP1-mCh
RNab-SNAPf
merge
E
merge
TOM20-GFP
GNab-SNAPf
merge
F
merge
LAMP1-GFP
GNab-SNAPf
merge

Figure 7.

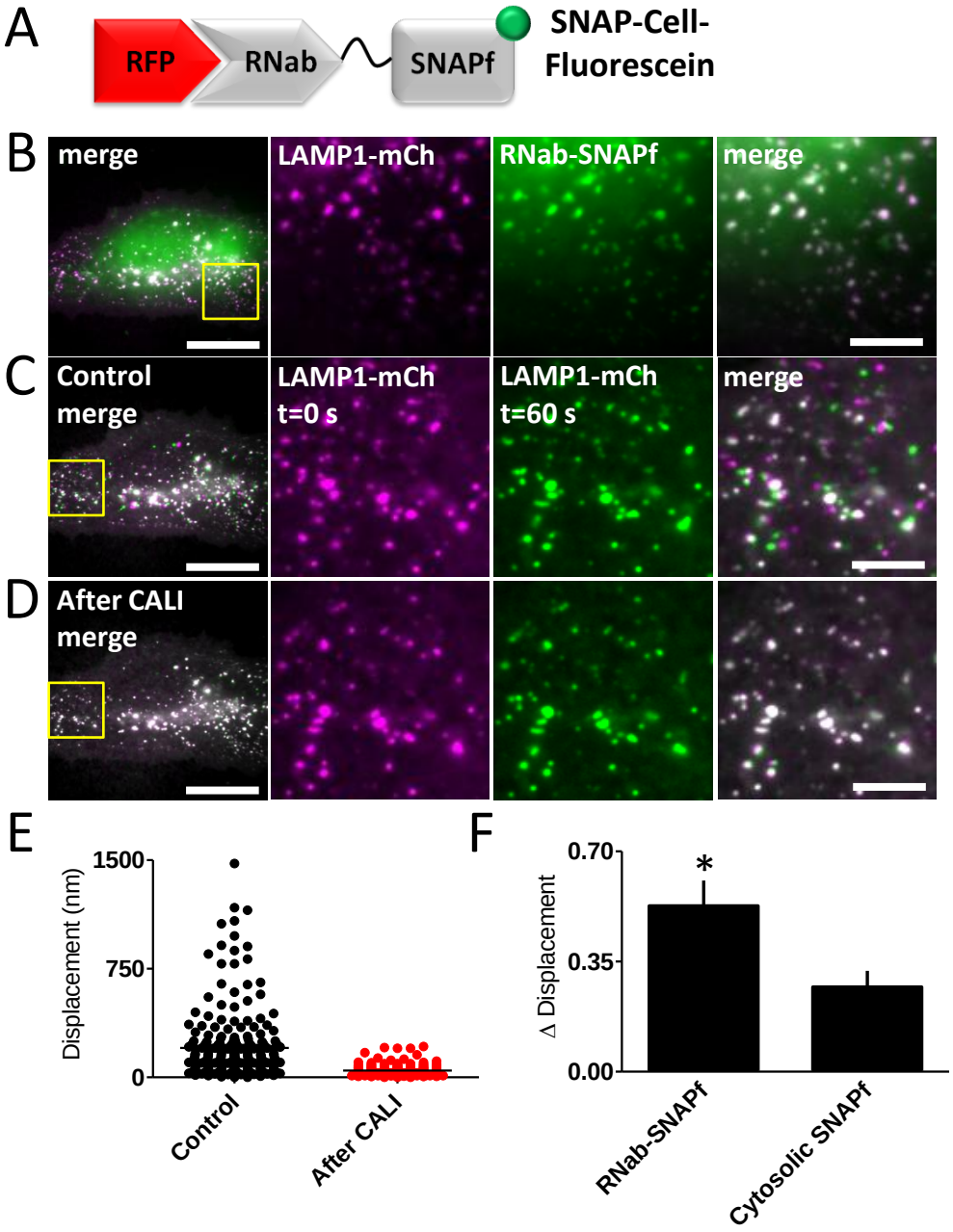
A
RFP
RNab
SNAPf
SNAP-Cell-
Fluorescein
B
merge
LAMP1-mCh
RNab-SNAPf
merge
C
Control
merge
LAMP1-mCh
t=0 s
LAMP1-mCh
t=60 s
merge
D
After CALI
merge
E
Displacement (nm)
1500
750
0
Control
After CALI
F
Δ Displacement
0.70
0.35
0.00
*
RNab-SNAPf
Cytosolic SNAPf

Figure 8.

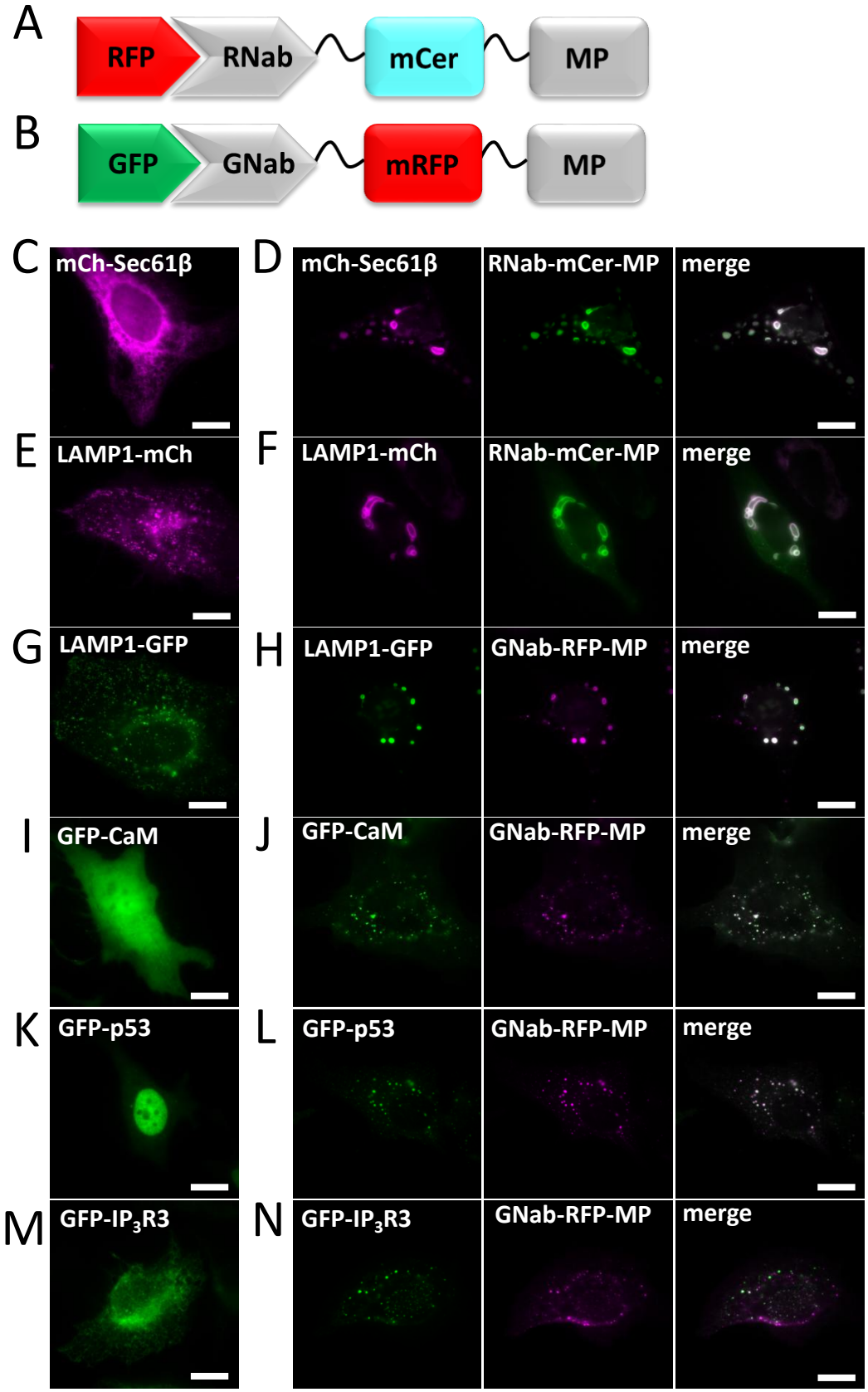
A
RFP
RNab
mCer
MP
B
GFP
GNab
mRFP
MP
C
mCh-Sec61β
D
mCh-Sec61β
RNab-mCer-MP
merge
E
LAMP1-mCh
F
LAMP1-mCh
RNab-mCer-MP
merge
G
LAMP1-GFP
H
LAMP1-GFP
GNab-RFP-MP
merge
I
GFP-CaM
J
GFP-CaM
GNab-RFP-MP
merge
K
GFP-p53
L
GFP-p53
GNab-RFP-MP
merge
M
GFP-IP3R3
N
GFP-IP3R3
GNab-RFP-MP
merge

Figure 9.

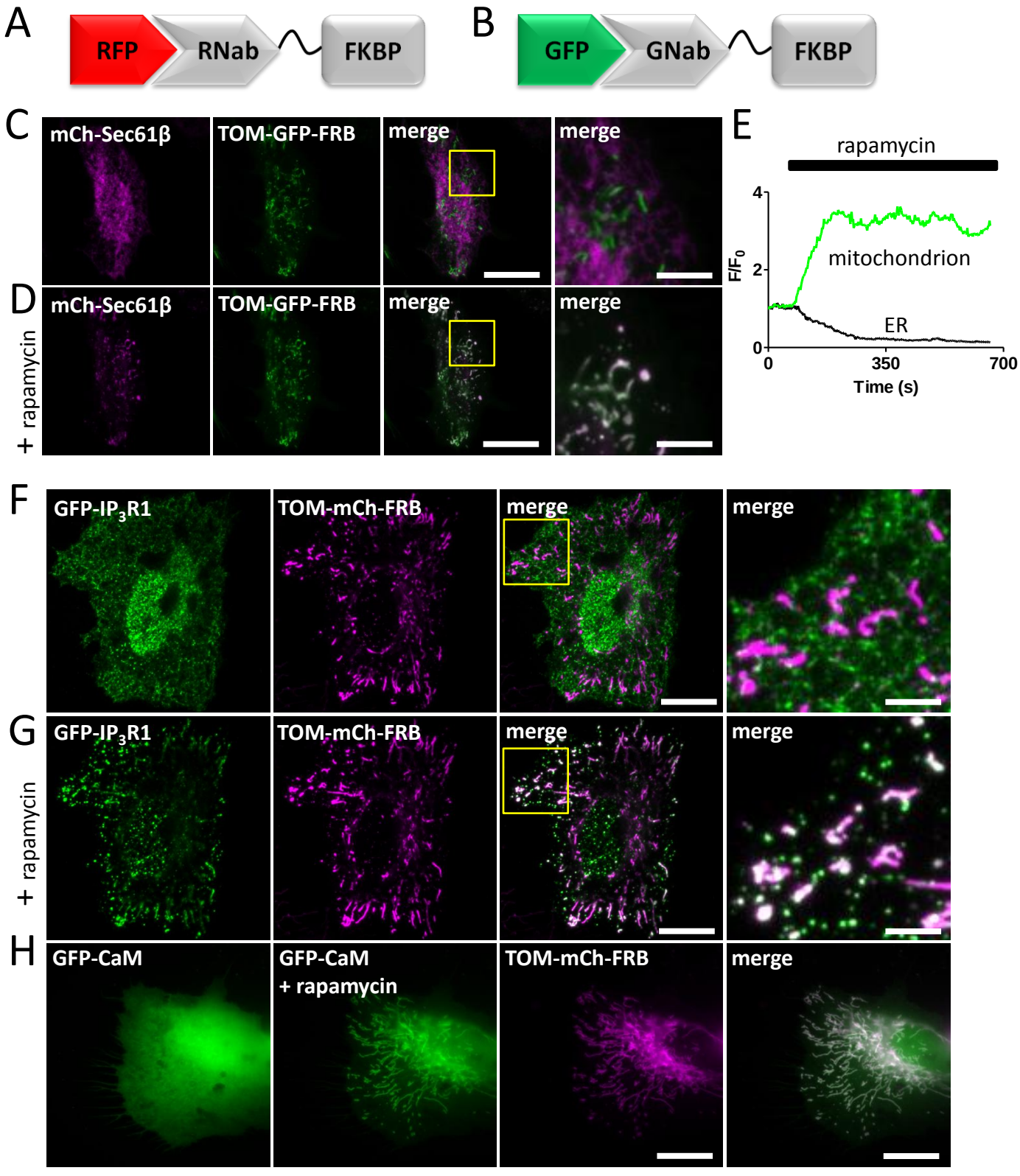
A
RFP
RNab
FKBP
B
GFP
GNab
FKBP
C
mCh-Sec61β
TOM-GFP-FRB
merge
merge
D
+ rapamycin
mCh-Sec61β
TOM-GFP-FRB
merge
merge
E
rapamycin
mitochondrion
ER
F/F0
4
2
0
0
350
700
Time (s)
F
GFP-IP3R1
TOM-mCh-FRB
merge
merge
G
+ rapamycin
GFP-IP3R1
TOM-mCh-FRB
merge
merge
H
GFP-CaM
GFP-CaM
+ rapamycin
TOM-mCh-FRB
merge

Figure 10.

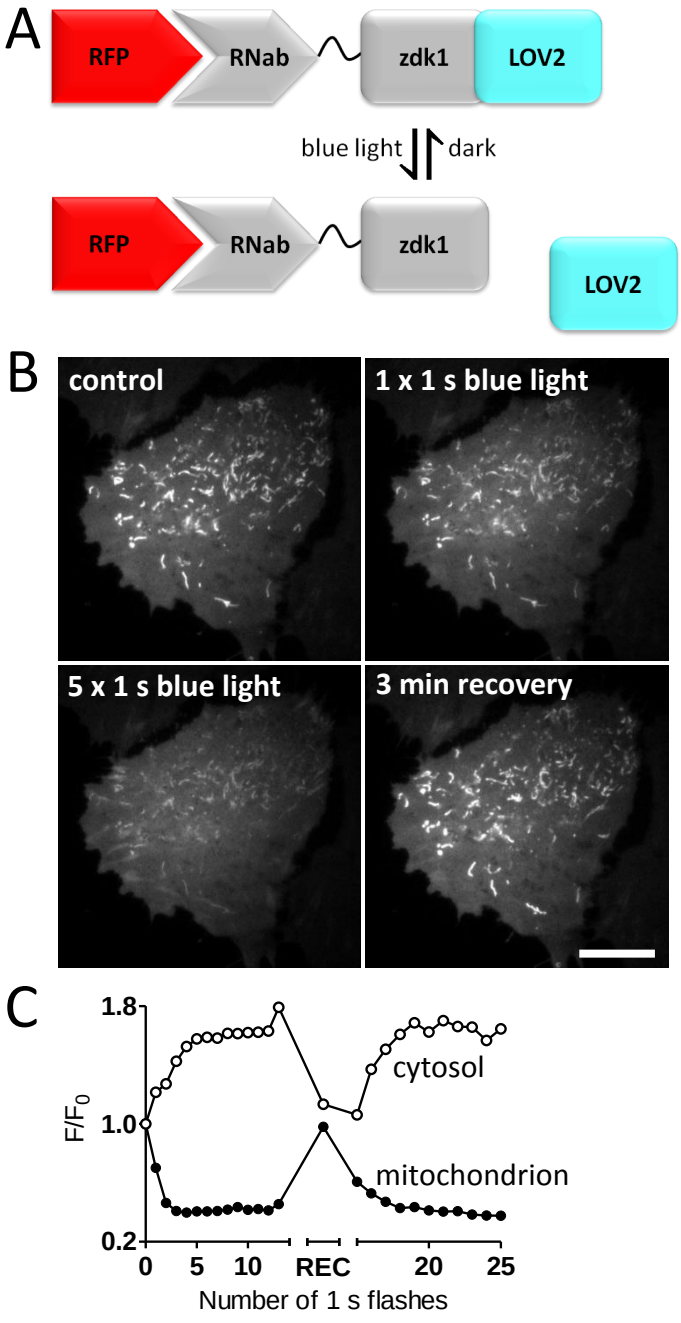
A
RFP
RNab
zdk1
LOV2
blue light
dark
RFP
RNab
zdk1
LOV2
B
control
1 x 1 s blue light
5 x 1 s blue light
3 min recovery
C
1.8
1.0
0.2
F/F0
cytosol
mitochondrion
0
5
10
REC
20
25
Number of 1 s flashes

Figure 11.

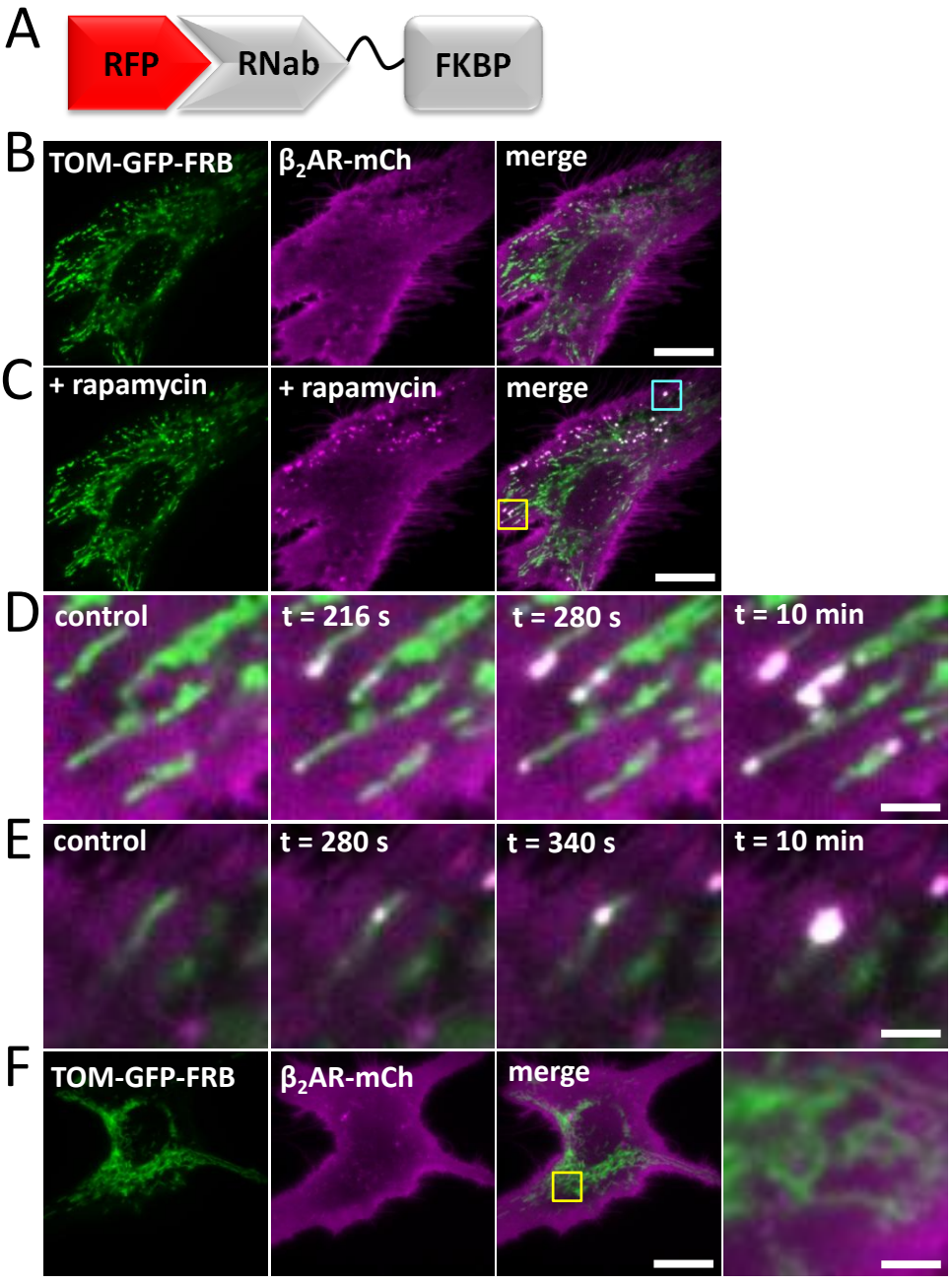
A
RFP
RNab
FKBP
B
TOM-GFP-FRB
β2AR-mCh
merge
C
+ rapamycin
+ rapamycin
merge
D
control
t = 216 s
t = 280 s
t = 10 min
E
control
t = 280 s
t = 340 s
t = 10 min
F
TOM-GFP-FRB
β2AR-mCh
merge

Figure 12.

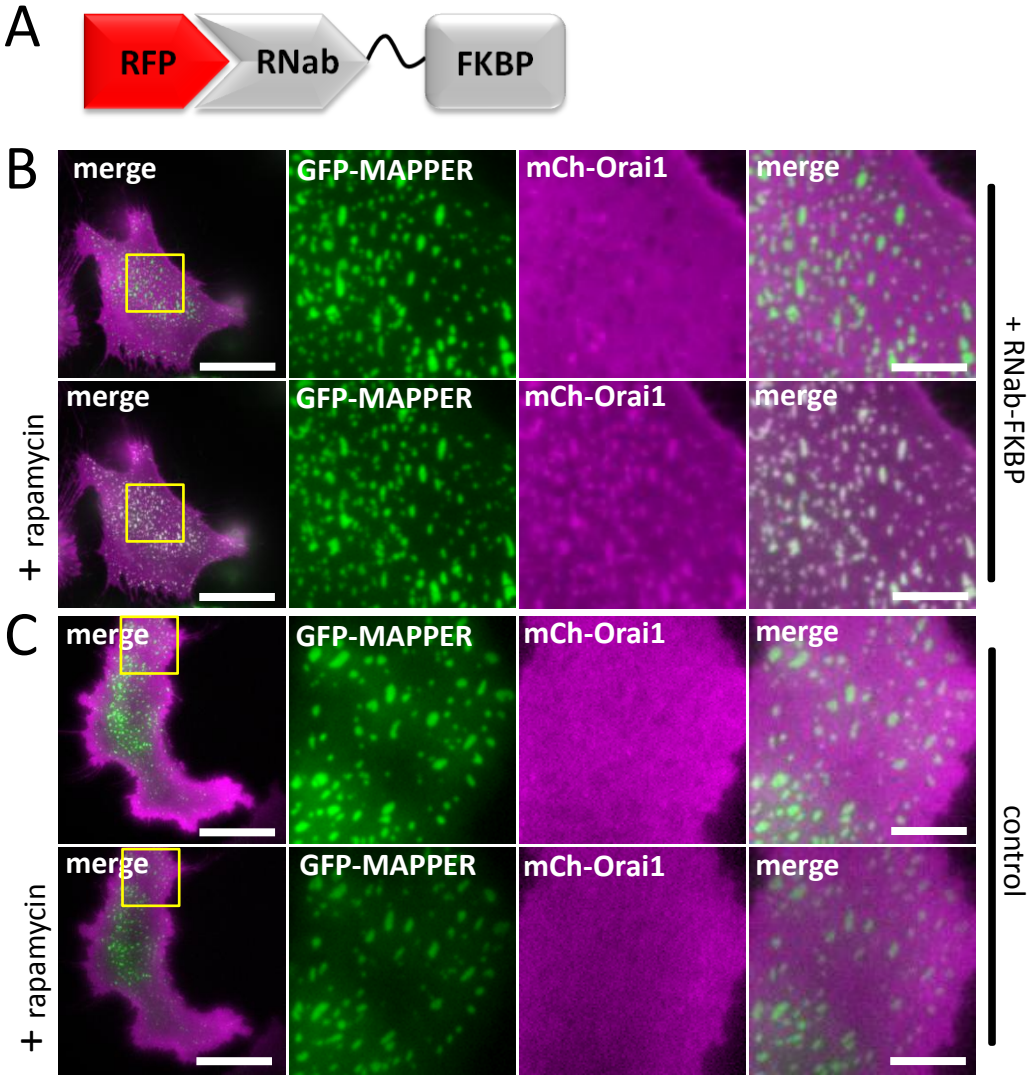
A
RFP
RNab
FKBP
B
merge
GFP-MAPPER
mCh-Orai1
merge
+ rapamycin
+ RNab-FKBP
C
control

Figure 13.

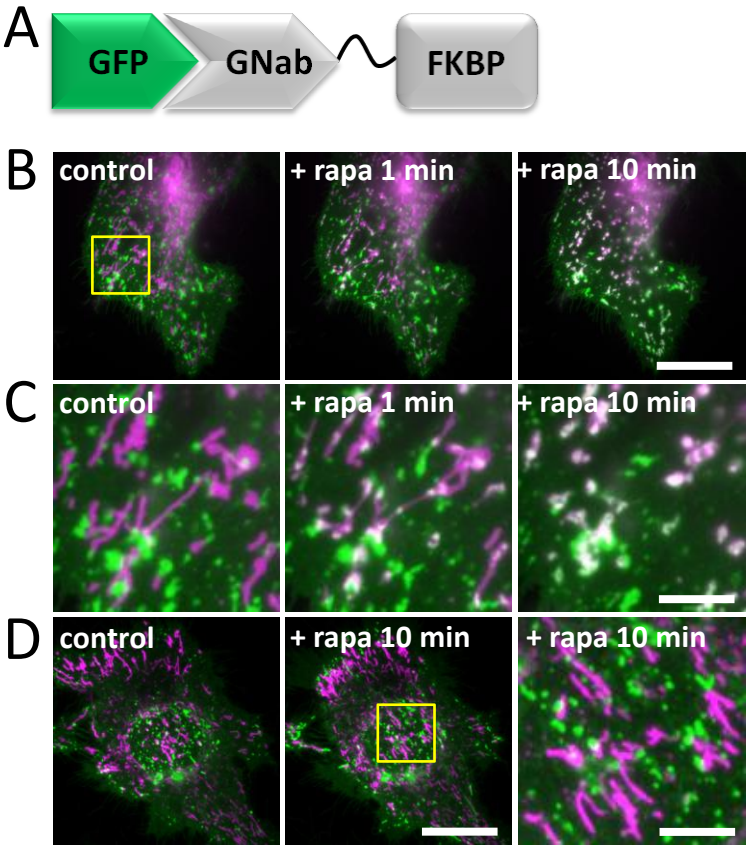
A
GFP
GNab
FKBP
B
control
+ rapa 1 min
+ rapa 10 min
C
control
+ rapa 1 min
+ rapa 10 min
D
control
+ rapa 10 min
+ rapa 10 min

Figure 14.

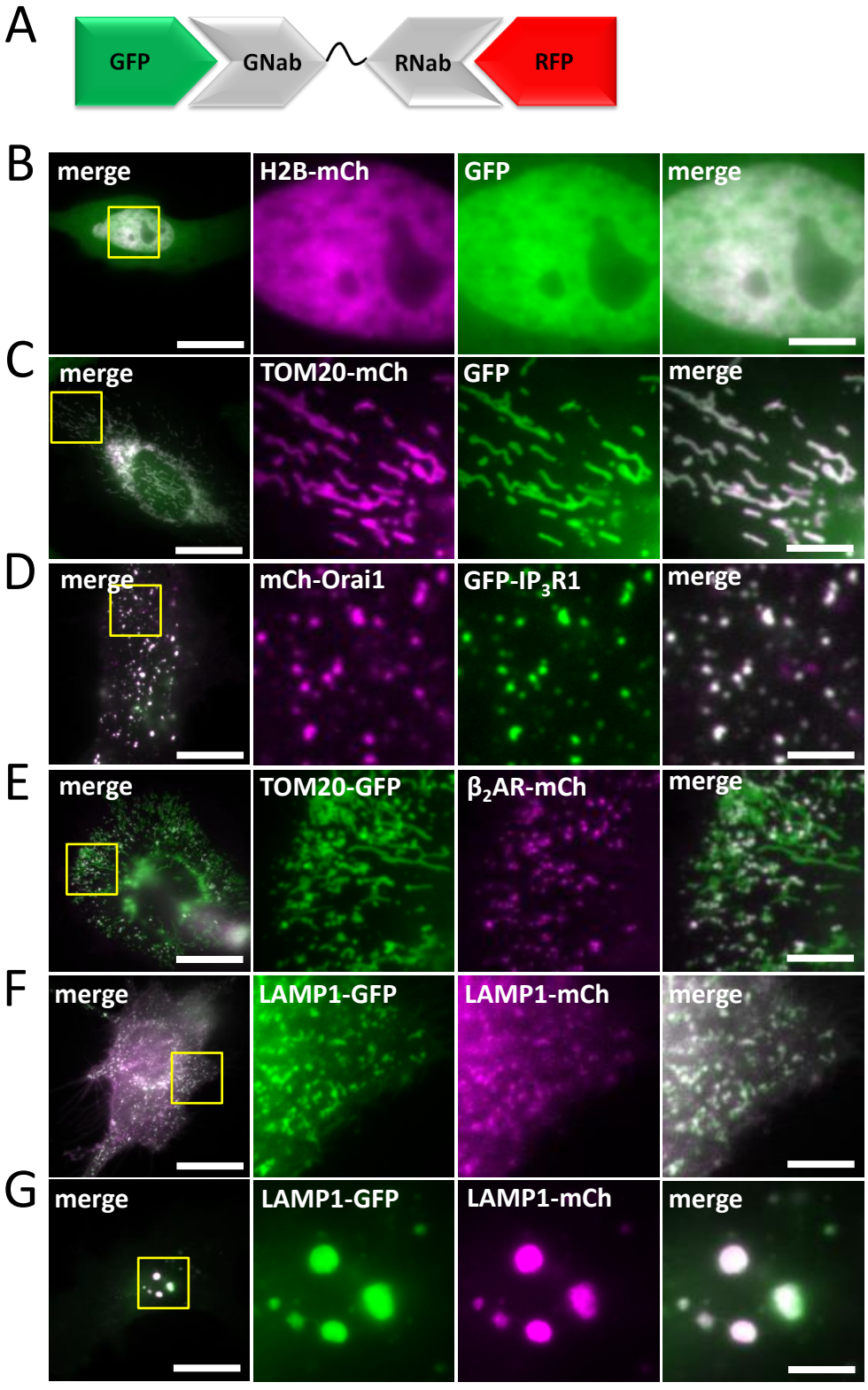
A
GFP
GNab
RNab
RFP
B
merge
H2B-mCh
GFP
merge
C
merge
TOM20-mCh
GFP
merge
D
merge
mCh-Orai1
GFP-IP3R1
merge
E
merge
TOM20-GFP
β2AR-mCh
merge
F
merge
LAMP1-GFP
LAMP1-mCh
merge
G
merge
LAMP1-GFP
LAMP1-mCh
merge

Figure 15.

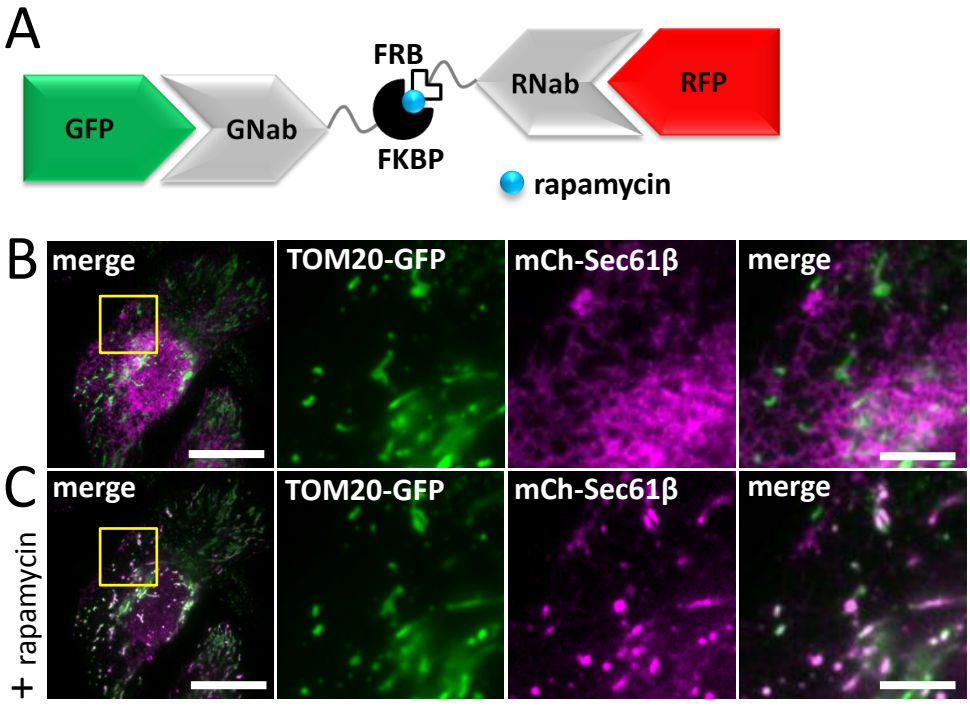
A
GFP
GNab
FRB
FKBP
RNab
RFP
rapamycin
B
merge
TOM20-GFP
mCh-Sec61β
merge
C
+ rapamycin
merge
TOM20-GFP
mCh-Sec61β
merge

Figure 16.

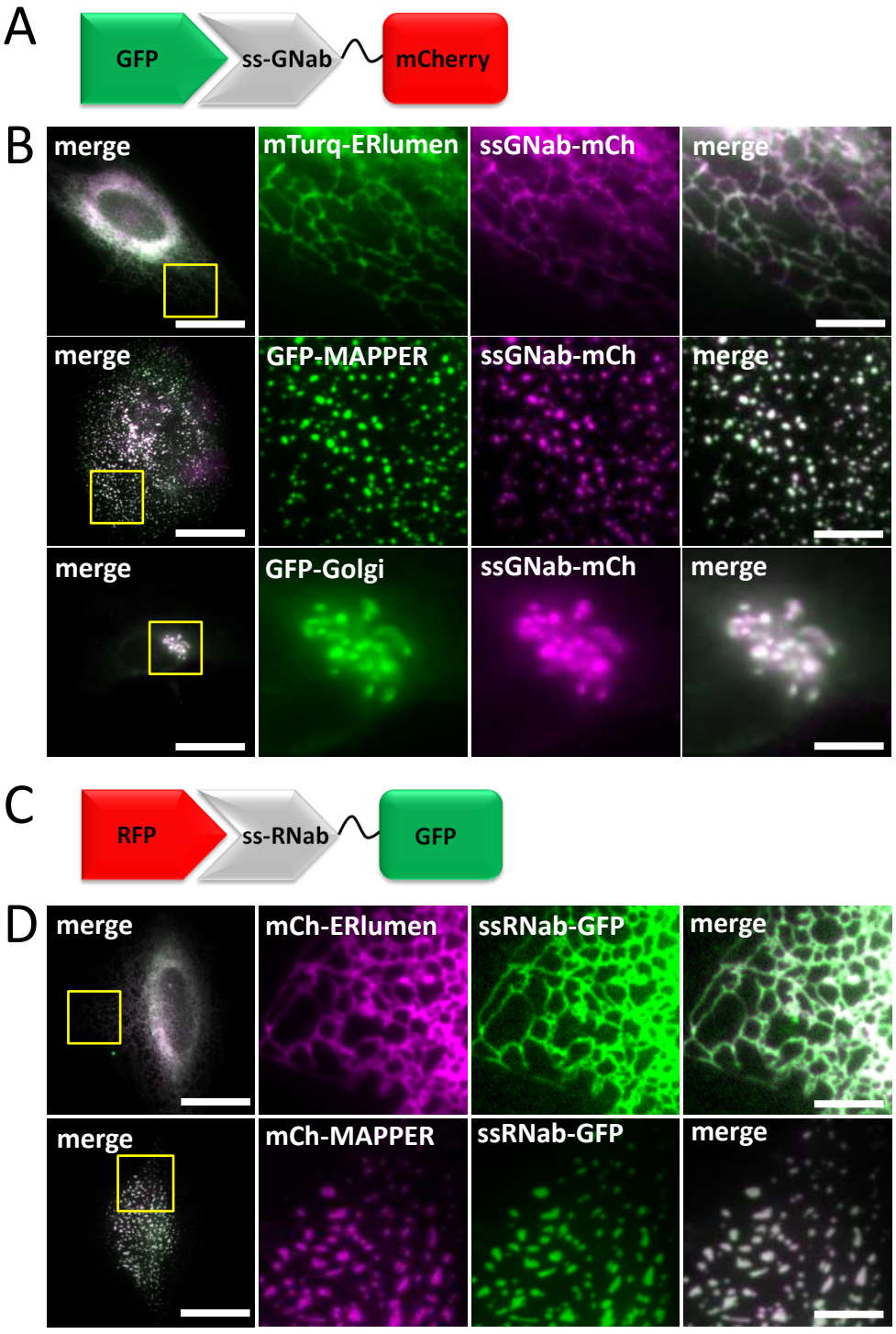
A
GFP
ss-GNab
mCherry
B
merge
mTurq-ERlumen
ssGNab-mCh
merge
merge
GFP-MAPPER
ssGNab-mCh
merge
merge
GFP-Golgi
ssGNab-mCh
merge
C
RFP
ss-RNab
GFP
D
merge
mCh-ERlumen
ssRNab-GFP
merge
merge
mCh-MAPPER
ssRNab-GFP
merge

Figure 17.

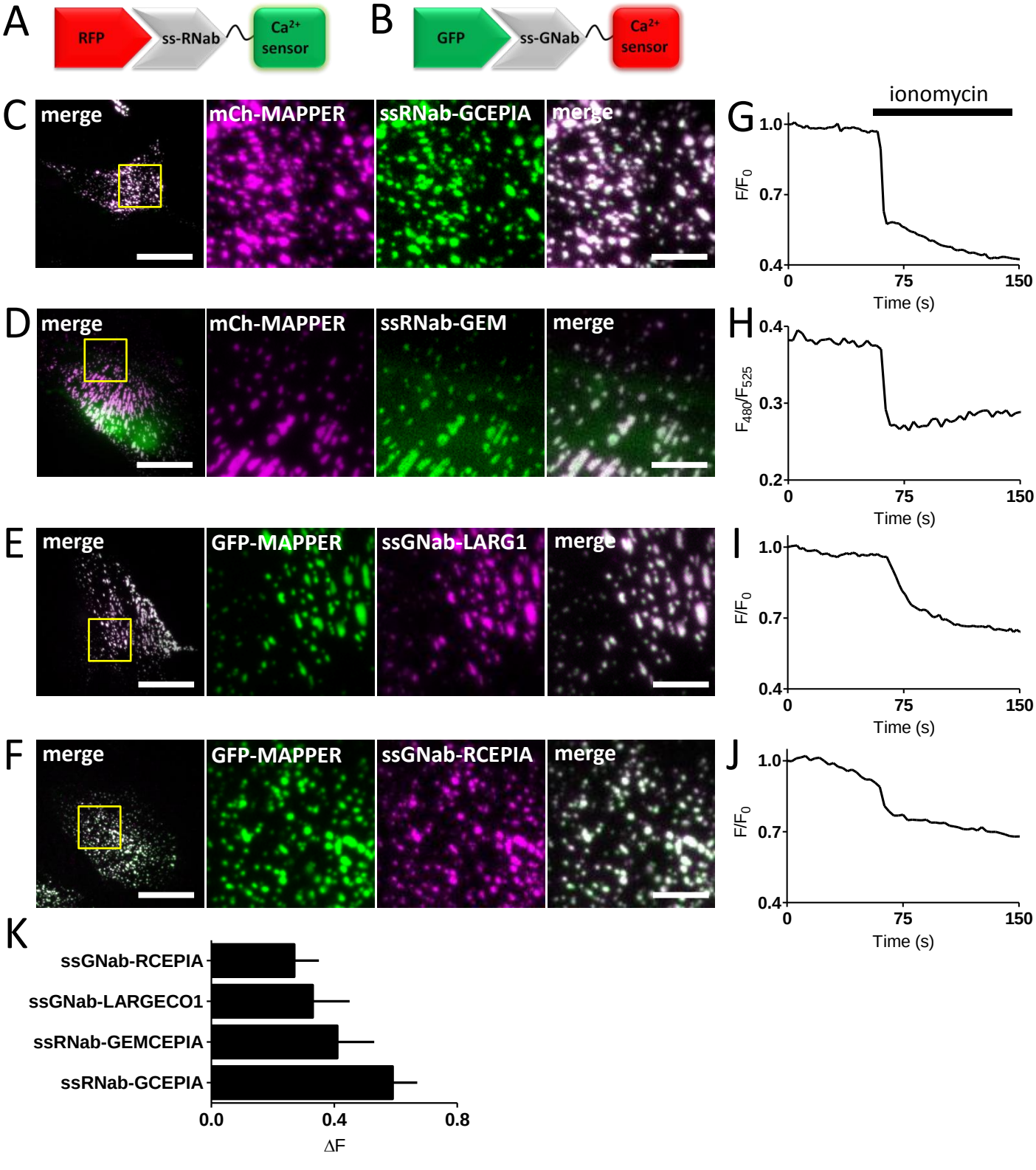
A
RFP
ss-RNab
Ca2+ sensor
B
GFP
ss-GNab
Ca2+ sensor
C
merge
mCh-MAPPER
ssRNab-GCEPIA
merge
D
merge
mCh-MAPPER
ssRNab-GEM
merge
E
merge
GFP-MAPPER
ssGNab-LARG1
merge
F
merge
GFP-MAPPER
ssGNab-RCEPIA
merge
G
ionomycin
F/F0
Time (s)
H
F480/F525
Time (s)
I
F/F0
Time (s)
J
F/F0
Time (s)
K
ssGNab-RCEPIA
ssGNab-LARGECO1
ssRNab-GEMCEPIA
ssRNab-GCEPIA
ΔF

Figure 18.